ferentiation. This study demonstrates that Cdk6 is a key molecule determining the differentiation rate of osteoblasts as a downstream effector of BMP-2/Smad signaling. Figure 7 depicts a schematic presentation of the mechanism by which BMP-2 induces osteoblast differentiation, as revealed by the present and previous studies. BMP-2 binds to the type II receptor and activates the type I receptor, leading to the formation of R-Smads/Co-Smad complexes, which are imported into the nucleus. The R-Smads/Co-Smad complexes then repress the *cdk6* promoter, thereby removing Cdk6-exerted blocking of differentiation.

The Cdk6-cyclin D3 complex is unique among cyclin D-cognate kinase combinations and evades inhibition by CKIs (8). Therefore, it can greatly enhance the proliferative potential of fibroblasts under growth-suppressive conditions and consequently sensitizes cells to physical and chemical transformation (2). This unique ability of Cdk6, however, does not seem to be responsible for the requirement of Cdk6 down-regulation for efficient osteoblast differentiation because we did not find any noticeable effect of BMP-2 and Cdk6 overexpression on the proliferation or even the cell cycle progression of MC3T3-E1 cells under the experimental conditions we employed. This apparent lack of a growth-stimulating function for Cdk6 in this cell line is consistent with the observation that Cdk4, but not Cdk6, was up-regulated by FGF-2, a potent stimulator of osteoblast proliferation.

The Rb protein has been implicated in osteoblast differentiation. The incidence of osteosarcoma increases 500-fold in patients inheriting *Rb* gene mutations. Recently, the Rb protein was reported to physically interact with Runx2/Cbfa1, which transactivates osteoblast-specific promoters (23). This transactivation is lost in tumor-derived Rb protein mutants, underscoring its potential role in osteoblast differentiation. The possibility that Rb directly mediates the role of Cdk6 as a differentiation inhibitor, however, is remote because unlike for Runx2/Cbfa1, there was no apparent correlation between the Cdk6-exerted differentiation block and the binding of Rb to the osteocalcin promoter.

How could Cdk6 control differentiation without influencing cell cycling? One possibility is that Cdk6 directly controls a factor(s) that is critically involved in differentiation. This possibility may not be as remote as is generally thought. In *Schizosaccharomyces pombe*, Pas1 cyclin and its partner kinase Pef1 activate a transcriptional factor complex that is functionally equivalent to E2F-DP of mammals, thereby promoting S-phase entry, just like Cdk6, yet they independently inhibit mating pheromone signaling, whose activation is essential for the differentiation of yeast cells (22). Thus, this may be a good model for the situation of Cdk6 in BMP-2-induced osteoblast differentiation, highlighting a potential functional similarity between Cdk6 and Pef1.

This study demonstrates for the first time that Cdk6, a G_1 cell cycle factor, plays a critical role in controlling BMP-2-invoked osteoblast differentiation. Several transcription factors, such as Runx2/Cbfa1, osterix, and low-density lipoprotein receptor protein 5, have been reported to be involved in bone formation (12, 16). Consequently, one of these factors may be responsible for the BMP-2-invoked repression of Cdk6 transcription. The identification of the transcriptional repressor as well as key targets of Cdk6 will definitely be required for a deeper understanding of the molecular basis of bone formation.

Finally, it is appropriate to stress that our finding is not specific to BMP-2-induced osteoblast differentiation. Very recently, Matushansky et al. reported a similar role for Cdk6 in the erythroid differentiation of a murine leukemia cell line (10).

ACKNOWLEDGMENTS

We thank Kohei Miyazono and Takeshi Imamura for kindly providing an adenovirus vector carrying *smad6* and Izumu Saito for an adenovirus vector carrying *lacZ*. We also thank H. Chikuda, M. Tsuji, and K. Baba for helpful discussion and support.

This work was supported by grants from the Department of Science, Education and Culture of Japan.

REFERENCES

1. **Bai, S., X. Shi, X. Yang, and X. Cao.** 2000. Smad6 as a transcriptional corepressor. J. Biol. Chem. 275:8267–8270.
2. **Chen, Q., J. Lin, S. Jinno, and H. Okayama.** 2003. Overexpression of Cdk6-cyclin D3 highly sensitizes cells to physical and chemical transformation. Oncogene 22:992–1001.
3. **Deng, C., P. Zhang, J. W. Harper, S. J. Elledge, and P. Leder.** 1995. Mice lacking p21CIP1/WAF1 undergo normal development, but are defective in G1 checkpoint control. Cell 82:675–684.
4. **DiChiara, M. R., J. M. Kiely, M. A. Gimbrone, Jr., M. E. Lee, M. A. Perrella, and J. N. Topper.** 2000. Inhibition of E-selectin gene expression by transforming growth factor beta in endothelial cells involves coactivator integration of Smad and nuclear factor kappaB-mediated signals. J. Exp. Med. 192:695–704.
5. **Hinds, P. W., and R. A. Weinberg.** 1994. Tumor suppressor genes. Curr. Opin. Genet. Dev. 4:135–141.
6. **Kretzschmar, M., and J. Massague.** 1998. SMADs: mediators and regulators of TGF-beta signaling. Curr. Opin. Genet. Dev. 8:103–111.
7. **Lee, K. S., H. J. Kim, Q. L. Li, X. Z. Chi, C. Ueta, T. Komori, J. M. Wozney, E. G. Kim, J. Y. Choi, H. M. Ryoo, and S. C. Bae.** 2000. Runx2 is a common target of transforming growth factor beta1 and bone morphogenetic protein 2, and cooperation between Runx2 and Smad5 induces osteoblast-specific gene expression in the pluripotent mesenchymal precursor cell line C2C12. Mol. Cell. Biol. 20:8783–8792.
8. **Lin, J., S. Jinno, and H. Okayama.** 2001. Cdk6-cyclin D3 complex evades inhibition by inhibitor proteins and uniquely controls cell's proliferation competence. Oncogene 20:2000–2009.
9. **Lopez-Rovira, T., E. Chalaux, J. L. Rosa, R. Bartrons, and F. Ventura.** 2000. Interaction and functional cooperation of NF-kappa B with Smads. Transcriptional regulation of the JunB promoter. J. Biol. Chem. 275:28937–28946.
10. **Matushansky, I., F. Radparvar, and A. I. Skoultchi.** 2003. CDK6 blocks differentiation: coupling cell proliferation to the block to differentiation in leukemic cells. Oncogene 22:4143–4149.
11. **Meyerson, M., G. H. Enders, C. L. Wu, L. K. Su, C. Gorka, C. Nelson, E. Harlow, and L. H. Tsai.** 1992. A family of human cdc2-related protein kinases. EMBO J. 11:2909–2917.
12. **Nakashima, K., X. Zhou, G. Kunkel, Z. Zhang, J. M. Deng, R. R. Behringer, and B. de Crombrugghe.** 2002. The novel zinc finger-containing transcription factor osterix is required for osteoblast differentiation and bone formation. Cell 108:17–29.
13. **Nakayama, K., N. Ishida, M. Shirane, A. Inomata, T. Inoue, N. Shishido, I. Horii, and D. Y. Loh.** 1996. Mice lacking p27(Kip1) display increased body size, multiple organ hyperplasia, retinal dysplasia, and pituitary tumors. Cell 85:707–720.
14. **Nevins, J. R.** 1992. E2F: a link between the Rb tumor suppressor protein and viral oncoproteins. Science 258:424–429.
15. **Nishimori, S., Y. Tanaka, T. Chiba, M. Fujii, T. Imamura, K. Miyazono, T. Ogasawara, H. Kawaguchi, T. Igarashi, T. Fujita, K. Tanaka, and H. Toyoshima.** 2001. Smad-mediated transcription is required for transforming growth factor-beta 1-induced p57(Kip2) proteolysis in osteoblastic cells. J. Biol. Chem. 276:10700–10705.
16. **Patel, M. S., and G. Karsenty.** 2002. Regulation of bone formation and vision by LRP5. N. Engl. J. Med. 346:1572–1574.
17. **Reddi, A. H.** 1998. Role of morphogenetic proteins in skeletal tissue engineering and regeneration. Nat. Biotechnol. 16:247–252.
18. **Sherr, C. J.** 1994. G1 phase progression: cycling on cue. Cell 79:551–555.
19. **Sherr, C. J., and J. M. Roberts.** 1999. CDK inhibitors: positive and negative regulators of G1-phase progression. Genes Dev. 13:1501–1512.
20. **Shi, X., X. Yang, D. Chen, Z. Chang, and X. Cao.** 1999. Smad1 interacts with homeobox DNA-binding proteins in bone morphogenetic protein signaling. J. Biol. Chem. 274:13711–13717.

21. **Takeda, K., H. Ichijo, M. Fujii, Y. Mochida, M. Saitoh, H. Nishitoh, T. K. Sampath, and K. Miyazono.** 1998. Identification of a novel bone morphogenetic protein-responsive gene that may function as a noncoding RNA. J. Biol. Chem. 273:17079–17085.
22. **Tanaka, K., and H. Okayama.** 2000. A Pcl-like cyclin activates the Res2p-Cdc10p cell cycle "start" transcriptional factor complex in fission yeast. Mol. Biol. Cell 11:2845–2862.
23. **Thomas, D. M., S. A. Carty, D. M. Piscopo, J. S. Lee, W. F. Wang, W. C. Forrester, and P. W. Hinds.** 2001. The retinoblastoma protein acts as a transcriptional coactivator required for osteogenic differentiation. Mol. Cell 8:303–316.
24. **Urano, T., H. Yashiroda, M. Muraoka, K. Tanaka, T. Hosoi, S. Inoue, Y. Ouchi, and H. Toyoshima.** 1999. p57(Kip2) is degraded through the proteasome in osteoblasts stimulated to proliferation by transforming growth factor beta1. J. Biol. Chem. 274:12197–12200.
25. **Verschueren, K., J. E. Remacle, C. Collart, H. Kraft, B. S. Baker, P. Tylzanowski, L. Nelles, G. Wuytens, M. T. Su, R. Bodmer, J. C. Smith, and D. Huylebroeck.** 1999. SIP1, a novel zinc finger/homeodomain repressor, interacts with Smad proteins and binds to 5′-CACCT sequences in candidate target genes. J. Biol. Chem. 274:20489–20498.
26. **Vidal, A., and A. Koff.** 2000. Cell-cycle inhibitors: three families united by a common cause. Gene 247:1–15.
27. **Wang, H., T. Goode, P. Iakova, J. H. Albrecht, and N. A. Timchenko.** 2002. C/EBPalpha triggers proteasome-dependent degradation of cdk4 during growth arrest. EMBO J. 21:930–941.
28. **Yan, Y., J. Frisen, M. H. Lee, J. Massague, and M. Barbacid.** 1997. Ablation of the CDK inhibitor p57Kip2 results in increased apoptosis and delayed differentiation during mouse development. Genes Dev. 11:973–983.
29. **Yoshida, Y., S. Tanaka, H. Umemori, O. Minowa, M. Usui, N. Ikematsu, E. Hosoda, T. Imamura, J. Kuno, T. Yamashita, K. Miyazono, M. Noda, T. Noda, and T. Yamamoto.** 2000. Negative regulation of BMP/Smad signaling by Tob in osteoblasts. Cell 103:1085–1097.
30. **Zhang, P., N. J. Liegeois, C. Wong, M. Finegold, H. Hou, J. C. Thompson, A. Silverman, J. W. Harper, R. A. DePinho, and S. J. Elledge.** 1997. Altered cell differentiation and proliferation in mice lacking p57KIP2 indicates a role in Beckwith-Wiedemann syndrome. Nature 387:151–158.
31. **Zhang, Y. W., N. Yasui, K. Ito, G. Huang, M. Fujii, J. Hanai, H. Nogami, T. Ochi, K. Miyazono, and Y. Ito.** 2000. A RUNX2/PEBP2alphaA/CBFA1 mutation displaying impaired transactivation and Smad interaction in cleidocranial dysplasia. Proc. Natl. Acad. Sci. USA 97:10549–10554.
32. **Zhu, H., P. Kavsak, S. Abdollah, J. L. Wrana, and G. H. Thomsen.** 1999. A SMAD ubiquitin ligase targets the BMP pathway and affects embryonic pattern formation. Nature 400:687–693.
33. **Zimmermann, M.** 1983. Ethical guidelines for investigations of experimental pain in conscious animals. Pain 16:109–110.BM

JOURNAL OF BONE AND MINERAL RESEARCH
Volume 19, Number 9, 2004
Published online on June 2, 2004; doi: 10.1359/JBMR.040515

SRC-1 Is Necessary for Skeletal Responses to Sex Hormones in Both Males and Females

Takashi Yamada,[1,2] Hirotaka Kawano,[1,2] Keisuke Sekine,[2] Takahiro Matsumoto,[2,3] Toru Fukuda,[2] Yoshiaki Azuma,[4] Keiji Itaka,[1] Ung-il Chung,[5] Pierre Chambon,[6] Kozo Nakamura,[1] Shigeaki Kato,[2,3] and Hiroshi Kawaguchi[1]

ABSTRACT: We created *SRC-1*$^{-/-}$ mice by mating floxed SRC-1 mice with CMV-Cre transgenic mice. The *SRC-1*$^{-/-}$ mice showed high turnover osteopenia under physiological conditions and hardly responded to osteoanabolic actions of exogenous androgen and estrogen in males and females, respectively, after gonadectomies, indicating that SRC-1 is essential for the maintenance of bone mass by sex hormones.

Introduction: Steroid receptor coactivator-1 (SRC-1) is the first identified coactivator of nuclear receptors. This study investigated the role of SRC-1 in skeletal tissues of males and females using the deficient (*SRC-1*$^{-/-}$) mice.
Materials and Methods: *SRC-1*$^{-/-}$ mice were generated by mating our original floxed SRC-1 mice with CMV-Cre transgenic mice. Bone metabolism between 24-week-old *SRC-1*$^{-/-}$ and wildtype (WT) littermates under physiological conditions was compared in males and females by radiological, histological, and biochemical analyses. Difference of skeletal responses to steroid hormones was examined by gonadectomies and exogenous administration experiments with the hormones. Statistical analysis was performed by ANOVA determined by posthoc testing using Bonferroni's method.
Results and Conclusions: Although *SRC-1*$^{-/-}$ mice showed no abnormality in growth or major organs, both males and females showed osteopenia with high bone turnover in the trabecular bones, but not in the cortical bones, compared with WT littermates. Their serum levels of sex hormones were upregulated, suggesting a compensatory reaction for the insensitivity to these hormones. Gonadectomies caused decreases in BMDs of *SRC-1*$^{-/-}$ and WT mice to the same levels; however, replacement with 5α-dihydrotestosterone and 17β-estradiol in males and females, respectively, failed to restore the bone loss in *SRC-1*$^{-/-}$, whereas the WT bone volume was increased to the sham-operated levels. In contrast, bone loss by administered prednisolone was similarly seen in *SRC-1*$^{-/-}$ and WT mice. We conclude that SRC-1 is essential for the maintenance of bone mass by sex hormones, but not for the catabolic action of glucocorticoid, under both physiological and pathological conditions.
J Bone Miner Res 2004;19:1452—1461. Published online on June 2, 2004; doi: 10.1359/JBMR.040515

Key words: **steroid hormone, coactivator, estrogen, androgen, glucocorticoid, bone**

INTRODUCTION

STEROID HORMONES ARE involved in mediating important physiological processes in numerous target tissues including breast, uterus, brain, and bone. The actions are mediated by their binding to structurally homologous nuclear receptors, which act as ligand-dependent transcription factors to either activate or repress target gene expression.[1–3] Among steroid hormones, the sex steroids estrogens and androgens are essential for normal skeletal development and maintenance of healthy bone remodeling during life.[4–7] Estrogen deficiency causes osteoporosis with high bone turnover in postmenopausal women, and this disorder can be prevented or reversed by estrogen replacement. Androgens are also known to exert beneficial effects on the maintenance of normal bone mass and remodeling. Patients with hypogonadism or androgen receptor (AR) defect often develop osteoporosis with high bone turnover, and testosterone supplementation can restore the BMD in eugonadal osteoporotic men.[8] Contrary to the bone-sparing actions of estrogens and androgens, another steroid hormone, glucocorticoids, stimulate bone resorption and inhibit bone formation in humans and consequently lead to a decrease in bone mass. Excess glucocorticoids in vivo, as a result of either prolonged steroid therapy or Cushing's syndrome, lead to the development of osteoporosis, the degree of which seems to be related to the duration and dose of treatment.[9,10]

Expressions of nuclear receptors of these steroid hormones, estrogen receptors (ERs), ARs, and glucocorticoid

The authors have no conflict of interest.

[1]Department of Orthopaedic Surgery, Faculty of Medicine, University of Tokyo, Tokyo, Japan; [2]Institute of Molecular and Cellular Biosciences, University of Tokyo, Tokyo, Japan; [3]SORST, Japan Science and Technology, Saitama, Japan; [4]Pharmacological Research Department, Teijin Co. Ltd., Tokyo, Japan; [5]Department of Tissue Engineering, Faculty of Medicine, University of Tokyo, Tokyo, Japan; [6]Institut de Genetique et de Biologie Moleculaire et Cellulaire, Universite Louis Pasteur, College de France, Strasbourg, France.

receptor (GRs), in bone have been identified mainly in osteoblasts and bone marrow cells.[4,5] The transcriptional activities of the receptors are mediated by interaction with several classes of coactivators/corepressors in a ligand-dependent manner.[11,12] The first characterized steroid receptor coactivator (SRC) family contains three homologous members: SRC-1, SRC-2 (also known as TIF2 and GRIP1), and SRC-3 (also known as p/CIP, AIB1, RAC3, ACTR, and TRAM-1).[13–16] The SRC coactivators have been reported to function in several ways: recruitment of histone acetyltransferases, histone methyltransferases, interaction with other coactivators, and contact with certain general transcription factors.[13] There are several pieces of evidence that the SRC coactivators play important roles clinically in mediating the response to steroid hormones. A chromosomal translocation that involves SRC-2 was identified in acute myeloid leukemia.[17] SRC-3 overexpression was documented in breast, ovarian, and pancreatic cancer.[18,19] These data suggest the possibility that the SRC family could modulate the response to steroid hormones in bone as well.

SRC-1 was originally cloned as a strong transactivator of GR[14] and has been reported to enhance the actions of many nuclear receptors, including ERs and AR.[13] Clinical involvement of SRC-1 has not yet been found; however, its in vivo function has been investigated by analyses of the *SRC-1*–deficient mice created by the O'Malley group using a conventional gene targeting method.[20] There were no apparent abnormalities in their major organs except for a partial resistance to sex hormones and thyroid hormone.[20–23] Aiming at generating double/triple mutant mice with tissue-specific *SRC-1* deficiency and other cofactor gene mutations such as SRC-2 and SRC-3 without embryonic lethality in the future, we first created floxed *SRC-1* mice in which the SRC-1 gene locus was flanked by loxP sites. In this study, the first using the floxed mice, we generated *SRC-1*–deficient (*SRC-1*$^{-/-}$) mice, whose SRC-1 function was generally blocked, by mating them with CMV-Cre transgenic mice. To define the functions of SRC-1 in skeletal tissues of both males and females, we analyzed the bone phenotype of the *SRC-1*$^{-/-}$ mice under physiological conditions and under stimulation by estrogens, androgens, or glucocorticoids.

MATERIALS AND METHODS

Generation of SRC-1$^{-/-}$ *mice*

Mouse SRC-1 genomic clones were obtained by screening an embryonic stem (ES) cell genomic library in λ phage (Stratagene) using human SRC-1 cDNA as a probe. A 20-kb fragment of mouse SRC-1 containing exons 3–5, encoding the basic-helix-loop-helix (bHLH) domain, was used to construct the targeting vector (Fig. 1A). The targeting vector consisted of a 7.7-kb 5′ homologous region containing exon 4, a 3.3-kb 3′ homologous region, a single loxP site, and the phosphoglycerate kinase-neomycin (PGKneo) cassette between the two loxP sites. The linearized targeting vector was electroporated into ES cells (25 μg/1.0 × 10^7 cells) using a Gene Pulser II (Bio-Rad Laboratories) at 250 V and 500 μF, and G418 neomycin-resistant clones were expanded as described previously.[24] Two ES cell clones (Fig. 1B, 4p29 and 4q30) containing a targeted *SRC-1L3* allele were identified by Southern blot analysis of *Eco*RI-digested ES cell genomic DNA, using 5′ (probe 1) and 3′ (probe 2) external probes and a neomycin probe. Targeted ES cells were aggregated with single eight-cell embryos from ICR mice (CLEA Japan) and returned to a pseudopregnant host of the same strain to generate chimeras as described previously.[24] Chimeric males were crossed with C57BL/6J females (CLEA Japan) to produce germ line transmission of the targeted *L3* allele. *SRC-1*$^{L3/L3}$ mice were then crossed with the CMV-Cre transgenic mice to generate *SRC-1*$^{L-/+}$ (also designated as *SRC-1*$^{+/-}$) mice (mice bearing one allele in which exon 4 and the neomycin cassette were deleted). Inbreeding of *SRC-1*$^{L-/+}$ mice yielded *SRC-1*$^{L-/L-}$ (also designated as *SRC-1*$^{-/-}$) mice homozygous for the deletion of SRC-1 exon 4. Because *SRC-1*$^{L3/L3}$ mice and CMV-Cre transgenic mice were in different strains, all *SRC-1*$^{-/-}$ mice used in this study had been backcrossed for 10 generations into the C57BL/6 background.

Animal conditions

All mice were kept in plastic cages under standard laboratory conditions with a 12-h dark, 12-h light cycle and a constant temperature of 23°C and humidity of 48%. The mice were fed a standard rodent diet (CE-2; CLEA Japan) containing 25.2% protein, 4.6% fat, 4.4% fiber, 6.5% ash, 3.44 kcal/g, 2.5 IU vitamin D_3/g, 1.09% calcium, and 0.93% phosphorus with water ad libitum. In each experiment, homozygous wildtype (WT) and *SRC-1*$^{-/-}$ mice that were littermates generated from the intercross between heterozygous mice were compared. All experiments were performed according to the protocol approved by the Animal Care and Use Committee of the University of Tokyo.

RT-PCR analysis

Total RNA was extracted from excised femora and tibias using an ISOGEN kit (Wako Pure Chemical Industries) and reverse transcribed using XL reverse transcriptase (Takara Shuzo Co.) and an oligo (dT) primer (Takara Shuzo Co.). After first-strand cDNA synthesis, 5% of the reaction mixture was amplified with r-*Taq*DNA polymerase (Takara Shuzo Co.) using specific primer pairs: 5′-CATGTAGGCCATGAGG TCCACCAC-3′ and 5′-TGAAGGTCGGTGTGAACGGATTTGGC-3′ for G3PDH; 5′-TACTGAGAAGAGGCGCAGGG-3′ and 5′-CCAGAAGAAGAGGGCCCAGC-3′ for SRC-1 (exon 4-exon 5); and 5′-ATGAGTGGCCTTGGGGACAG-3′ and 5′-CCAGAAGAAGAGGGCCCAGC-3′ for SRC-1 (exon 3-exon 5). Up to 35 cycles of amplification were performed, with each cycle consisting of 96°C for 30 s, 55°C for 60 s, and 72°C for 60 s.

Western blot analysis

To detect SRC-1 protein expression, bone cell lysates were separated by SDS-PAGE and transferred onto nitrocellulose membranes. Membranes were probed with a goat polyclonal antibody raised against a carboxyl terminus peptide of human SRC-1 that is identical to the corresponding mouse sequence (1:1000 dilution, C-20; Santa Cruz Biotechnology) and a rabbit polyclonal antibody raised against a recombinant protein corresponding to amino acids 350–

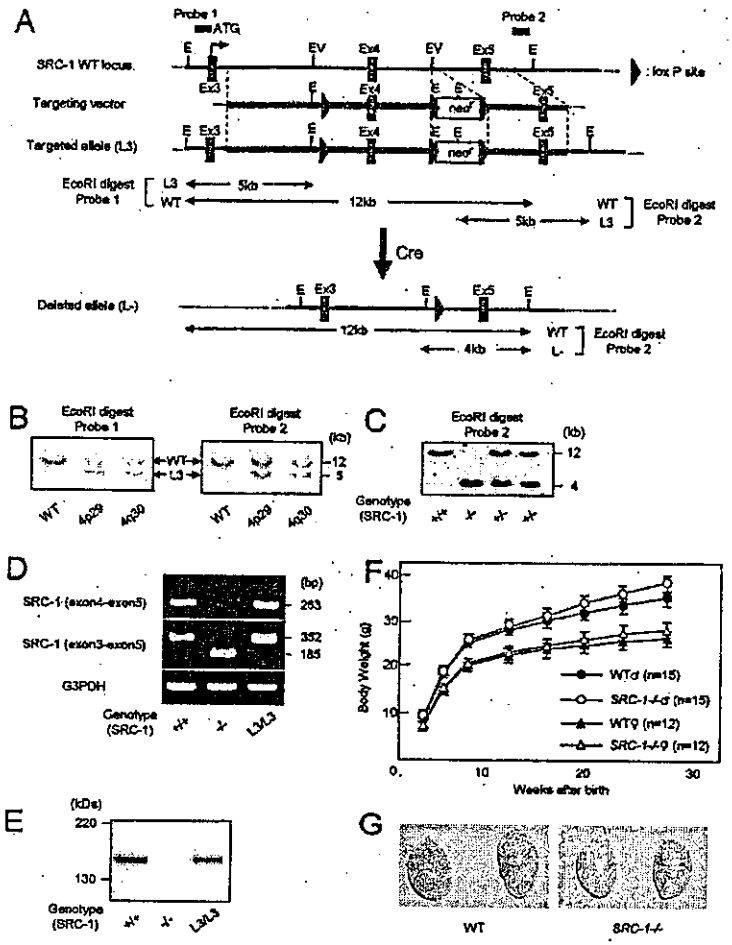

FIG. 1. Targeted disruption of mouse *SRC-1* gene. (A) Strategy to generate *SRC-1*$^{-/-}$ mice showing the WT SRC-1 locus, the targeting vector, the targeted allele (*L3*), and the deleted allele (*L−*) obtained after Cre-mediated excision. Exons (Ex) are shown as shaded boxes. The location of probes 1 and 2 are indicated. E, *Eco*RI; EV, *Eco*RV; neo^r, PGKneo cassette. LoxP sites are indicated as black arrowheads. (B) Southern blot analysis of targeted ES clones. Genomic DNA from WT ES cells and homologous targeted clones (4p29 and 4q30) were digested with *Eco*RI for hybridization with probe 1 (left) and 2 (right). (C) Southern blot analysis of offspring of heterozygous mates with probe 2. (D) Detection of the SRC-1 transcript by RT-PCR in long bones of WT, *SRC-1*$^{-/-}$, and floxed *SRC-1* (*SRC-1*$^{L3/L3}$) mice. (E) Western blot analysis of the SRC-1 protein using an antibody against a carboxyl terminus of the SRC-1 peptide in long bones of WT, *SRC-1*$^{-/-}$, and floxed *SRC-1* (*SRC-1*$^{L3/L3}$) mice. (F) Growth curves determined by the body weight of WT and *SRC-1*$^{-/-}$ mice in both sexes. Data are expressed as means (symbols) ± SE (error bars) for 15 mice/group for males and 12 mice/group for females. There were no significant differences between WT and *SRC-1*$^{-/-}$ mice in either sex ($p > 0.05$). (G) Smaller testes were observed in male *SRC-1*$^{-/-}$ mice.

690 mapping within an internal region of SRC-1 of mouse origin (1:1000 dilution, M-341; Santa Cruz Biotechnology) and then a peroxidase-conjugated second antibody. Blots were visualized using an ECL detection kit (Amersham Biosciences).

Radiological analysis

Bone radiographs of excised femora, tibias, and the fifth lumbar vertebrae from 12-, 16-, and 24-week-old WT and *SRC-1*$^{-/-}$ littermates were taken using a soft X-ray apparatus (model CMB-2; SOFTEX). BMD was measured by DXA using a bone mineral analyzer (PIXImus Mouse Densitometer; GE Medical Systems). CT was performed with a pQCT analyzer (XCT Research SA+; Stratec Medizintecnik) operating at a resolution of 80 μm. Metaphyseal pQCT scans of femora were performed to measure the trabecular volumetric BMD. The scan was positioned in the metaphysis at 1.2 mm proximal from the distal growth plate. This area contains cortical as well as trabecular bone. The trabecular bone region was defined by setting the threshold to 395 mg/cm^3 according to a previous report.[25] Mid-diaphyseal pQCT scans of femora were performed to determine the cortical volumetric BMD and the cortical thickness. The mid-diaphyseal region of femora in mice contains mostly cortical bone. The cortical bone region was defined by setting the threshold to 690 mg/cm^3.[25] The interassay CVs for the pQCT measurements were <2%. μCT scanning of the fifth lumbar vertebrae was performed using a composite X-ray analyzer (model NX-CP-C80H-IL; Nittetsu ELEX Co.), and a total of 300 cross-sectional tomograms per vertebra were obtained with a slice thickness of 10 μm and reconstructed at 12 × 12 pixels into a 3D feature by the volume-rending method (software, VIP-Station; Teijin System Technology) using a computer (model SUN SPARK-5; Sun Microsystems). Electronic sections were cut in the transverse, coronal, and sagittal planes on 3D reconstructed images.

Histological analysis

Histological analyses were performed using 24-week-old WT and *SRC-1*$^{-/-}$ littermates. For von Kossa and toluidine blue stainings, lumbar vertebrae were fixed with 70% ethanol, embedded in glycol methacrylate without decalcification, and sectioned in 3-μm slices using a microtome (model 2050; Reichert Jung). For calcein double labeling,

mice were injected subcutaneously with 16 mg/kg body weight of calcein at 10 and 3 days before death. Sections with toluidine blue stainings were used to visualize calcein labels under fluorescent light microscopy. $TRACP^+$ cells were stained at pH 5.0 in the presence of L(+)-tartaric acid using naphthol AS-MX phosphate (Sigma-Aldrich Co.) in *N,N*-dimethyl formamide as the substrate. The specimens were subjected to histomorphometric analyses using a semi-automated system (Osteoplan II; Carl Zeiss), and measurements were made at 400× magnification. Parameters for the trabecular bone were measured in an area 0.3 mm in length from the cortical bone at the fifth lumbar vertebrae. Nomenclature, symbols, and units are those recommended by the Nomenclature Committee of the American Society for Bone and Mineral Research.[26]

Serum and urinary biochemistry

Blood samples from 24-week-old WT and *SRC-1*$^{-/-}$ littermates (n = 15/genotype for males and n = 12/genotype for females) were collected by heart puncture under Nembutal (Dainippon Pharmaceutical Co.) anesthesia, and urine samples were collected for 24 h before death using oil-sealed bottles in metabolism cages (CL-0305; CLEA Japan). The levels of calcium, phosphorus, and alkaline phosphatase activity in serum were measured using a calcium HR kit (Wako Pure Chemical Industries), an inorganic phosphorus II kit (Wako Pure Chemical Industries), and a liquitech alkaline phosphatase kit (Roche Diagnostics), respectively, with an autoanalyzer (type 7170; Hitachi Hith-Technologies). Serum osteocalcin levels were measured using the competitive radioimmunoassay (RIA) kit (Biomedical Technologies). Serum testosterone and 17β-estradiol (E_2) levels were measured using RIA kits (Diagnostic Products), and serum leptin was assayed with the ELISA-based Quantikine M mouse leptin immunoassay kit (R&D Systems). Urinary deoxypyridinoline was measured using the Pyriliks-D ELISA (Metra Biosystems). The values were corrected according to urinary creatinine (Cr), as measured by a standard colorimetric technique with an autoanalyzer (type 7170).

Gonadectomy and hormone treatment

Male WT and *SRC-1*$^{-/-}$ littermates were orchidectomized or sham-operated at 16 weeks of age and implanted subcutaneously with 60-day time-release pellets (Innovative Research of America) containing either placebo or 5α-dihydrotestosterone (DHT; 10 mg/pellet; 8 mice/group). Female WT and *SRC-1*$^{-/-}$ littermates were ovariectomized or sham-operated at 16 weeks of age and implanted subcutaneously with 60-day time-release pellets containing either placebo or E_2 (0.025 mg/pellet; 8 mice/group). For the glucocorticoid experiment, male WT and *SRC-1*$^{-/-}$ littermates were implanted subcutaneously with 60-day time-release pellets containing either placebo or prednisolone (4 mg/pellet) at 16 weeks of age (8 mice/group). BMD of the fifth lumbar vertebrae was measured in situ by DXA using a bone mineral analyzer (PIXImus Mouse Densitometer) at 16 and 24 weeks. All mice were killed at 24 weeks of age, seminal vesicles of male and uteri of female mice were excised and weighed, and BMD of the excised fifth lumbar vertebrae was measured by DXA.

Statistical analysis

All data are expressed as means ± SE. Means of groups were compared by ANOVA, and significance of differences was determined by posthoc testing using Bonferroni's method.

RESULTS

Generation of SRC-1$^{-/-}$ *mice by a Cre-loxP system*

We targeted exon 4 of the *SRC-1* gene, which encodes the bHLH domain to generate functionally null SRC-1 mutant mice (Fig. 1A). The targeting vector was designed with three loxP sites flanking exon 4 and the PGKneo cassette. Complete excision of exon 4 and floxed PGKneo cassette in the *L3* allele mediated by Cre recombinase was confirmed in the genomic DNA sequence of F_2 offspring, and the mutation resulted in the creation of a stop codon at exon 5 by splicing exon 3 and 5 transcripts. Thus, the truncated protein produced from the deleted allele lacks the C-terminal region that includes all SRC-1 functional domains for transcriptional activation, histone acetyltransferase activity, and interactions with nuclear receptors, CBP, P300, and p/CAF.[14,27,28]

Chimeric males derived from targeted L3 ES clones transmitted the mutation through their germline, yielding floxed *SRC-1* (*SRC-1*$^{L3/L3}$) mice. Floxed *SRC-1* mice grew normally and exhibited no overt abnormalities with normal SRC-1 mRNA and protein expression levels (Figs. 1D and 1E). Floxed *SRC-1* mice were crossed with CMV-Cre transgenic mice to generate SRC-1 heterozygous (*SRC-1*$^{+/-}$) mice. Inbreeding of heterozygous *SRC-1*$^{+/-}$ mice yielded *SRC-1*$^{-/-}$ mice in accordance with Mendelian expectations (Fig. 1C). Short SRC-1 transcripts exclusive of exon 4 were detected by RT-PCR in the long bones of *SRC-1*$^{-/-}$ mice (Fig. 1D); however, because of the creation of a stop codon at exon 5, no SRC-1 protein expression was shown by Western blot analysis using an antibody against a carboxyl terminus of the SRC-1 peptide, confirming disruption of the *SRC-1* gene (Fig. 1E). Similar mRNA and protein expression patterns were observed in tissues including liver, kidney, isolated primary osteoblasts, and bone marrow cells, even when we used other primer sets and antibodies (data not shown).

Both male and female *SRC-1*$^{-/-}$ mice grew normally and were apparently indistinguishable from WT littermates. Growth curves determined by the body weight were somewhat similar between WT and *SRC-1*$^{-/-}$ mice in both males and females during the observation period up to 28 weeks, although a slight increase of body weight caused by obesity was seen in both sexes of *SRC-1*$^{-/-}$ mice as they got older (Fig. 1F). While no abnormality of reproductive organs, including ovary and uterus, was found in female *SRC-1*$^{-/-}$ mice, a slight hypoplasia of testis was seen (~20% in weight) in males (Fig. 1G). These abnormalities were the same as those reported in the *SRC-1*–deficient mice generated by a conventional method.[20]

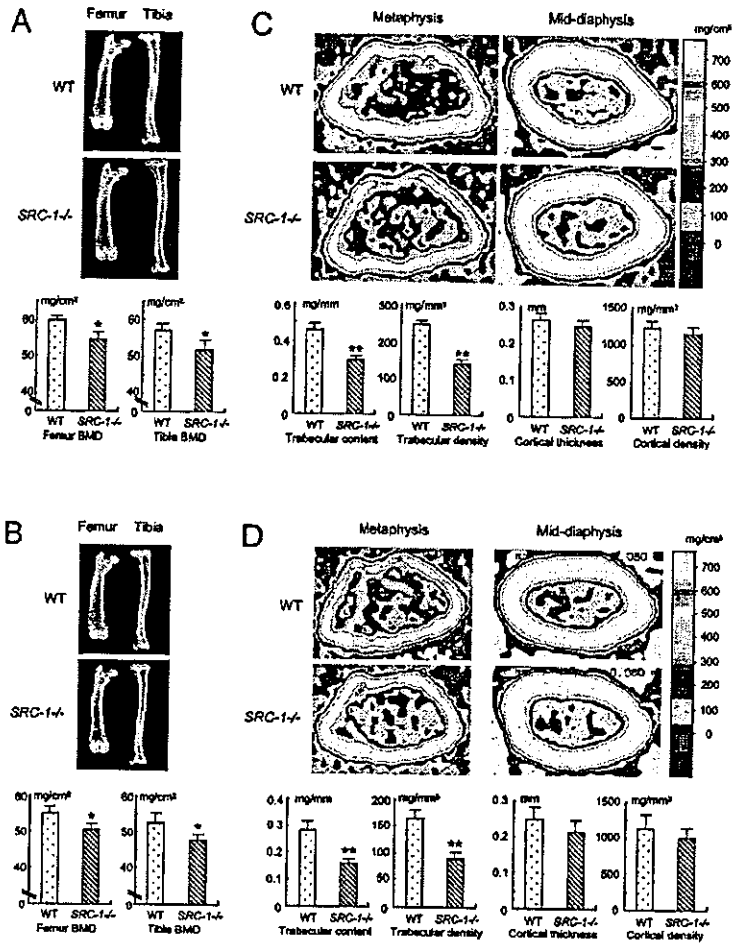

FIG. 2. Radiological findings of the long bones in *SRC-1*$^{-/-}$ and WT littermates. (A and B) Plain X-ray images of femur and tibia in representative (A) males and (B) females of both genotypes at 24 weeks of age. The BMD of the entire femurs and tibias measured by DXA is shown in the graphs below. (C and D) pQCT images of the distal metaphysis (left) and the mid-diaphysis (right) of the femurs in representative (C) males and (D) females of both genotypes at 24 weeks of age. The color gradient indicating BMD is shown in the right bars. The trabecular content and density at the metaphysis and the cortical thickness and density at the mid-diaphysis are shown in the graphs below. Data in all graphs are expressed as means (bars) ± SE (error bars) for 15 mice/group for males and 12 mice/group for females. Significant difference from WT: $*p < 0.05$, $**p < 0.01$.

Osteopenia in male and female SRC-1$^{-/-}$ *mice*

To learn the physiological role of SRC-1 in skeletal tissues, we analyzed the long bones and vertebrae of *SRC-1*$^{-/-}$ mice. The lengths of the long bones and the trunk of these mice were similar to those of WT littermates, at least during the observation period up to 24 weeks of age, indicating that SRC-1 is not involved in the regulation of skeletal growth. BMD was similar between long bones of the two genotypes at 12 weeks of age and tended to be lower in *SRC-1*$^{-/-}$ than WT mice at 16 weeks, although this was not statistically significant (data not shown). At 24 weeks, however, *SRC-1*$^{-/-}$ mice showed ~10% less BMD of long bones than WT littermates in males (Fig. 2A) and females (Fig. 2B). When trabecular and cortical bones were analyzed separately in the femora using pQCT, *SRC-1*$^{-/-}$ mice showed ~35–45% lower BMC and BMD of trabecular bones; however, the cortical bones were not affected by the SRC-1 deficiency in either males (Fig. 2C) or females (Fig. 2D).

To investigate the abnormalities of the *SRC-1*$^{-/-}$ trabecular bones in more detail, we performed morphological analyses of vertebral bodies that are rich in trabecular bone in males and females at 24 weeks of age. 3D CT analysis of the fifth lumbar vertebrae confirmed the decrease in *SRC-1*$^{-/-}$ trabecular bone in both sexes (Fig. 3).

Histomorphometric analyses confirmed that the bone volumes (BV/TV) were decreased by 30–40% in the *SRC-1*$^{-/-}$ males and females compared with those of WT littermates (Table 1). Parameters for both bone formation (Ob.S/BS, MAR, and BFR) and resorption (N.Oc/B.Pm, Oc.S/BS, and ES/BS) were also significantly higher in *SRC-1*$^{-/-}$ mice. The increase in bone resorption parameters (~60–80%) exceeded that in bone formation parameters (~30–60%), indicating a state of high-turnover osteopenia that is characteristic of osteoporosis with sex hormone deficiency.

Biochemical markers in the serum and urine supported the increase of bone turnover by SRC-1 deficiency (Table 2). Bone formation markers (serum alkaline phosphatase and osteocalcin) and a bone resorption marker (urinary deoxypyridinoline) were higher in both males and females of *SRC-1*$^{-/-}$ mice than those in WT littermates. The serum calcium and phosphorus levels were similar between the two genotypes, suggesting that the skeletal abnormalities by SRC-1 deficiency were not the result of the changed calcium or phosphorus levels. Considering that *SRC-1*$^{-/-}$ mice

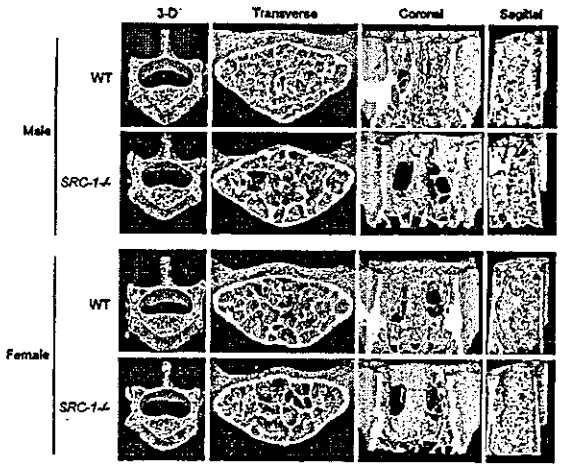

FIG. 3. Radiological and histological findings of the lumbar vertebrae in *SRC-1*$^{-/-}$ and WT littermates. 3D CT images of the fifth vertebrae in representative males and females of both genotypes at 24 weeks of age. The BMD of the entire fifth vertebrae measured by DXA was 58.7 ± 3.5 (male WT), 49.0 ± 2.1 (male *SRC-1*$^{-/-}$), 48.7 ± 3.3 (female WT), and 41.6 ± 1.4 mg/cm^2 (female *SRC-1*$^{-/-}$) for 15 mice/group for males and 12 mice/group for females. There were significant differences between WT and *SRC-1*$^{-/-}$ in both sexes ($p < 0.05$).

showed a slight obesity at this age, we measured the serum level of leptin, which has recently been reported to be an antiosteogenic factor. The level was somewhat upregulated, although not significantly, in *SRC-1*$^{-/-}$ mice. Interestingly, despite the high bone turnover, the serum levels of both testosterone in males and estradiol in females were elevated in *SRC-1*$^{-/-}$ mice, suggesting a compensatory mechanism in the endocrine system for the insensitivity to these sex hormones.

Insensitivity to administration of sex hormones in gonadectomized SRC-1$^{-/-}$ *mice*

To examine the involvement of SRC-1 in the skeletal actions of sex hormones, we performed hormone administration experiments (Figs. 4A–4D). After orchidectomy and ovariectomy on males and females, respectively, at 16 weeks of age, a slow-releasing pellet of sex hormone or placebo was subcutaneously implanted, and BMD was measured at 24 weeks. Effects of gonadectomies and hormone replacements were confirmed by seminal vesicle and uterine weights of males and females, respectively (Table 3). Both orchidectomy and ovariectomy markedly decreased these weights in WT and *SRC-1*$^{-/-}$ mice. DHT and E_2 restored them to the levels similar to those of sham-operated mice in WT, whereas these hormones restored almost one-half of them in *SRC-1*$^{-/-}$ mice, which is consistent with a previous study using another *SRC-1* knockout mouse.[20] Regarding BMD, besides the raw BMD values (Figs. 4A and 4C), the percent changes from baseline to final BMD during 8 weeks (Figs. 4B and 4D) were also compared between WT and *SRC-1*$^{-/-}$ mice. Both orchidectomy and ovariectomy decreased bone volumes of the two genotypes to the same levels in both sexes (~45.0 mg/cm^2 in males and 38.5 mg/cm^2 in females). When slow-releasing pellets of DHT and E_2 were subcutaneously implanted in the gonadectomized males and females, respectively, they prevented bone loss in WT mice. However, these hormone replacements restored little of the bone loss in *SRC-1*$^{-/-}$ mice, indicating that SRC-1 deficiency impairs the skeletal responses to sex hormones in both males and females.

We further examined the contribution of SRC-1 to the catabolic action of glucocorticoids on bone (Figs. 4E and 4F). When a slow-releasing pellet of prednisolone was implanted at 16 weeks, BMD was reduced similarly in WT and *SRC-1*$^{-/-}$ littermates, ~10% during the following 8 weeks, suggesting that SRC-1 is not essential in the bone catabolic action of glucocorticoids mediated by GR.

DISCUSSION

In this study, we originally generated *SRC-1*$^{-/-}$ mice by means of a Cre-loxP system and confirmed the lack of *SRC-1* gene expression in bone and other tissues. There is another *SRC-1* knockout mouse line that was generated by the O'Malley group, using a conventional gene targeting method.[20] Because both our *SRC-1*$^{-/-}$ mice and the conventional *SRC-1* knockout mice have similar genetic backgrounds by being extensively backcrossed into C57BL/6, we assume that the two mice should exhibit similar phenotypes. Modder et al.[29] recently reported skeletal phenotypes of the conventional *SRC-1* knockout mice showing resistance to the osteoanabolic action of estradiol in ovariectomized females, which is consistent with our results. Comparison of the two knockout mice is summarized in Table 4. In the conventional knockout mice, the targeting event inserted an in-frame stop codon at the Met (381) in exon 11, causing the downstream deletion of genomic sequence. Although the RNA encoding the bHLH-PAS domain was normally expressed in the knockout mice, all SRC-1 functional domains for transcriptional activation were confirmed to be disrupted, and it was not likely to have a dominant negative effect, because the bHLH-Per-Arnt-Sim (PAS) domain interacted with neither the full-length SRC-1 nor other SRC-1 family members such as TIF2.[20] In our *SRC-1*$^{-/-}$ mice, a stop codon created in the middle of the bHLH-PAS domain at exon 5 predicts a truncated product that is shorter than that in the conventional *SRC-1* knockout mice. Besides the skeletal finding in female mice in the previous report,[29] this study revealed that the SRC-1 deficiency also caused resistance to osteoanabolic action of androgen in orchidectomized males and no abnormality in osteocatabolic action of glucocorticoids. Discrepancy between the previous and present studies seems to be the bone phenotype under physiological conditions: their conventional *SRC-1* knockout mice did not exhibit osteopenia, whereas our *SRC-1*$^{-/-}$ mice did. We believe, however, that this discrepancy is caused by the difference in age when the analyses were done: 12 weeks for them versus 24 weeks for us. In fact, our study also did not detect significant difference of BMD at 12 weeks between WT and *SRC-1*$^{-/-}$ littermates of either sex under physiological conditions. It is speculated that, with aging, the compensatory elevation of

TABLE 1. HISTOMORPHOMETRY OF TRABECULAR BONE OF LUMBAR VERTEBRAE

	BV/TV (%)	*Ob.S/BS (%)*	*MAR (μm/day)*	*BFR (μm³/μm²/day)*	*N.Oc/B.Pm (/100 mm)*	*Oc.S/BS (%)*	*ES/BS (%)*
Male							
WT	16.48 ± 2.09	6.27 ± 0.63	0.94 ± 0.19	0.08 ± 0.02	94.24 ± 11.31	2.10 ± 0.15	3.45 ± 0.49
SRC-1$^{-/-}$	11.53 ± 1.39*	9.15 ± 0.81*	1.40 ± 0.15*	0.13 ± 0.02	159.05 ± 12.02†	3.50 ± 0.21†	5.73 ± 0.57†
Female							
WT	12.97 ± 0.65	8.55 ± 0.51	1.02 ± 0.11	0.11 ± 0.01	109.66 ± 12.64	2.41 ± 0.19	3.72 ± 0.25
SRC-1$^{-/-}$	7.73 ± 0.95†	11.02 ± 1.32	1.42 ± 0.08*	0.18 ± 0.03*	174.95 ± 24.39*	4.28 ± 0.31†	6.47 ± 0.21†

Parameters for the trabecular bone were measured in an area 0.3 mm in length from cortical bone at the fifth lumbar vertebrae in toluidine blue and calcein double-labeled sections. Data are expressed as means ± SEM (n = 15/group for males and n = 12/group for females). BV/TV, trabecular bone volume expressed as a percentage of total tissue volume; Ob.S/BS, percentage of bone surface covered by cuboidal osteoblasts; MAR, mineral apposition rate; BFR, bone formation rate expressed by MAR × percentage of bone surface exhibiting double labels plus one half single labels; N.Oc/B.Pm, number of mature osteoclasts in 10 cm of bone perimeter; Oc.S/BS, percentage of bone surface covered by mature osteoclasts; ES/BS, percentage of eroded surface.
*$p < 0.05$; †$p < .01$; significantly different from WT mice.

TABLE 2. SERUM AND URINARY BIOCHEMISTRY

	Serum							*Urine*
	ALP (IU/liter)	*Osteocalcin (ng/ml)*	*Ca (mg/dl)*	*P (mg/dl)*	*Leptin (ng/ml)*	*Testosterone (ng/ml)*	*17β-estradiol (pg/ml)*	*DPD (nM/mM Cr)*
Male								
WT	78.16 ± 6.91	20.61 ± 1.76	7.93 ± 0.21	7.52 ± 0.49	6.01 ± 0.74	2.45 ± 0.33	2.34 ± 0.21	8.29 ± 0.42
SRC-1$^{-/-}$	99.67 ± 8.16*	26.42 ± 2.16*	8.11 ± 0.18*	7.51 ± 0.57	7.45 ± 0.57	3.41 ± 0.42*	2.78 ± 0.28	11.31 ± 0.1†
Female								
WT	90.22 ± 5.74	25.05 ± 1.62	8.04 ± 0.11	7.18 ± 0.29	6.87 ± 0.67	ND	5.18 ± 0.57	9.32 ± 0.19
SRC-1$^{-/-}$	117.13 ± 7.72*	33.34 ± 1.41†	7.87 ± 0.19	7.15 ± 0.41	8.18 ± 1.24	ND	7.12 ± 0.64*	12.71 ± 0.28†

Data are expressed as means ± SEM (n = 15/group for males and n = 12/group for females). *ALP*, alkaline phosphatase; *Ca*, calcium; *P*, phosphorus; *DPD*, deoxypyridinoline; ND, not detected.
Concentration of *DPD* was collected according to urinary creatinine concentration.
*$p < 0.05$; †$p < 0.01$; significantly different from WT mice.

sex hormone levels through a feedback mechanism becomes too weak to catch up with the decreased sensitivity to these hormones by the SRC-1 deficiency.

Administration experiments with steroid hormones revealed that the SRC-1 deficiency caused resistance to osteoanabolic actions of sex hormones in gonadectomized male and female mice. More interesting is that *SRC-1*$^{-/-}$ mice exhibited osteopenia under physiological conditions at 24 weeks, suggesting a bone-sparing role of endogenous SRC-1. This is also likely to be caused by the impairment of actions of endogenous sex hormones on bone for the following reasons. First, morphological and biochemical analyses revealed that *SRC-1*$^{-/-}$ mice exhibited the decrease in trabecular bone with a high turnover state, which is characteristic of the pathology of sex hormone deficiencies. Second, the serum sex hormone levels were upregulated in *SRC-1*$^{-/-}$ mice of both sexes, implicating a compensatory reaction for the insensitivity to them. Third, in the absence of sex hormones by gonadectomies, the BMD decreased to similar levels between WT and *SRC-1*$^{-/-}$ mice. These results indicate that the SRC-1 function is essential for the maintenance of bone mass by sex hormones under both physiological and pathological conditions.

In males, as well as activating the AR, androgens can be converted into estrogens by the enzyme aromatase,[30] and therefore can exert their effects not only through the AR, but also through the ERs. Because DHT cannot be converted to estrogens by aromatase, loss of the osteoanabolic effect of exogenous DHT in *SRC-1*$^{-/-}$ orchidectomized male mice can be interpreted as a defect in AR, but not ER, signaling. Furthermore, we and others recently revealed that the androgen/AR signaling is indispensable for male-type bone remodeling, independent of the estrogen/ER signaling, by the analysis of AR-deficient mice.[31,32] Under physiological conditions, however, there are many reports showing the essential contribution of the estrogen/ER signaling to male bones. Inhibition of aromatase activity in male rats impairs bone remodeling and mimics the effect of orchidectomy,[33,34] and the aromatase-deficient mice develop osteopenia.[35] Two men with mutations in the *aromatase P450* gene exhibited delayed skeletal maturation and osteopenia, despite high levels of circulating androgens and the ability to respond to estradiol.[36,37] These observations are similar to those seen in a man with a mutation in the ER,[38] reinforcing the importance of the estrogen/ER signaling in male bones. In addition, the SRC-1 transcriptional activation of AR is known to be much weaker than that of ERs.[39] Therefore, the bone loss seen in *SRC-1*$^{-/-}$ males may, at least in part, be caused by impairment of the

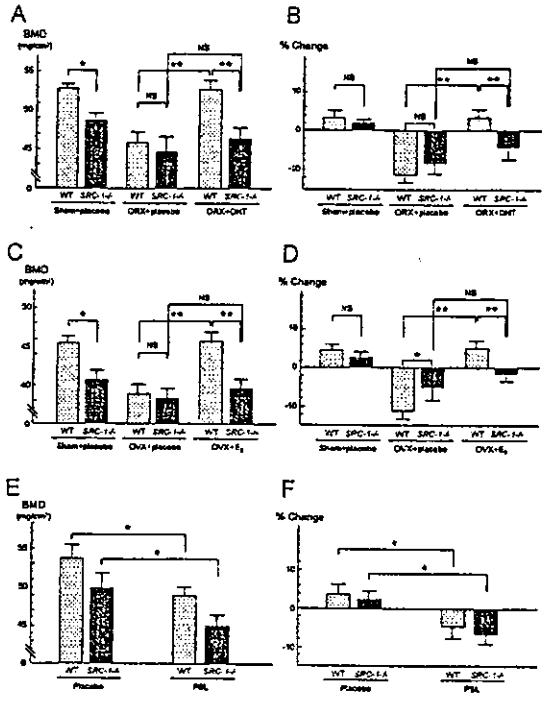

FIG. 4. Effects of gonadectomy and hormone administrations on BMD of vertebrae in *SRC-1*$^{-/-}$ and WT littermates. (A and B) Male WT and *SRC-1*$^{-/-}$ littermates were orchidectomized or sham-operated at 16 weeks of age and implanted subcutaneously with slow-releasing pellets containing either placebo or DHT (10 mg/pellet). At 16 and 24 weeks of age, BMD of the fifth lumbar vertebrae was measured by DXA. (C and D) Female WT and *SRC-1*$^{-/-}$ littermates were ovariectomized or sham-operated at 16 weeks of age and implanted subcutaneously with slow-releasing pellets containing either placebo or E_2 (0.025 mg/pellet). BMD was measured as described above. (E and F) Male WT and *SRC-1*$^{-/-}$ littermates without operation were implanted subcutaneously with slow-releasing pellets containing either placebo or prednisolone (PSL; 4 mg/pellet) at 16 weeks of age. BMD was measured as described above. Both the (A, C, and E) raw BMD values of the excised vertebrae at 24 weeks and (B, D, and F) the percent changes of BMD of the vertebrae measured in situ during 8 weeks were compared between WT and *SRC-1*$^{-/-}$ mice. Data in all graphs are expressed as means (bars) ± SE (error bars) for 8 mice/group. Significant difference: $*p < 0.05$, $**p < 0.01$. NS, not significant ($p > 0.05$).

estrogen/ER signaling, as well as of the androgen/AR signaling.

It is interesting that SRC-1 deficiency caused the decrease of trabecular bone but not of cortical bone. Similar findings are reported in a study using the conventional *SRC-1* knockout mice.[29] A previous study examining ERα and ERβ expressions by immunohistochemistry in neonatal human ribs showed that trabecular bone contains both ERs, whereas only ERα was detected in cortical bone.[40] Modder et al.[29] also showed that the cancellous bone of the mouse vertebrae contains both ERs, whereas the cortical bone of the mouse femur contains exclusively ERα. In addition, another recent study revealed that, in osteoblastic cells, SRC-1 potentiates the transcriptional activity of co-expressed ERα/ERβ or ERβ alone, with little or no potentiation of ERα.[41] Hence, as Modder et al.[29] stated in their report, at least in females, the discrepancy of the SRC-1 contribution between trabecular and cortical bone may be caused by the relative expression of ERα versus ERβ in the two kinds of bone and to the specific interactions of SRC-1 with these receptor isoforms in bone cells. In males as well, difference of effects on the two kinds of bone can be explained by the distinctions of expression and activation of the ER isoforms, because estrogen/ER signaling is important in male bone, as described above. Regarding AR, its distribution in the trabecular and cortical bones remains unknown. Further studies on the expression and the interaction with SRC-1 of AR and ERs will elucidate the clinical importance of SRC-1 in human bones.

The conventional *SRC-1* knockout mice are reported to be obesity prone under a high-fat diet.[42] In this study as well, our *SRC-1*$^{-/-}$ mice, fed a standard diet, showed higher body weight and serum leptin levels compared with those of WT littermates, although both were slight and not statistically significant. A series of recent reports showed that leptin, an anorexigenic hormone secreted by adipocytes, also shows antiosteogenic action centrally through hypothalamic and sympathetic nervous systems.[43] However, this low level of increase in the leptin level seems inadequate to explain the significant bone loss by the SRC-1 deficiency. In addition, the *SRC-1*$^{-/-}$ bone exhibited high bone turnover with stimulated bone formation, which is the opposite of leptin action.

Nuclear receptors exert their tissue-specific function using different coactivator/corepressor complexes ingeniously and appropriately in each tissue.[11,12,44] Therefore, it is possible that not only the dysfunction of nuclear receptors or their ligands, but also that of the cofactors, leads to various disorders. The function of cofactors might explain the difference among individuals in the sensitivity to hormones and related agents as well. Despite important roles of sex hormones in bone, the effect of their gain or loss of function varies widely among individuals, and this has not yet been fully explained by analyses of the receptor levels. Accumulated genetic studies have failed to identify a definite association of the ER or AR gene polymorphisms with BMD.[45] Furthermore, a case of testicular feminization in a patient without an AR gene mutation was reported as a possible co-factor disease.[46] From the results of this study, SRC-1 may be a strong candidate that regulates the variety of the pathophysiology of sex hormone-deficient osteoporosis and therapeutic effects of hormone replacements in humans, because humans are known to be more sensitive to sex hormone deficiency than mice.

ACKNOWLEDGMENTS

We thank Dr Yasuji Yamamoto (Taiho Pharmaceutical Co., Ltd.) for helpful discussion and Kaori Yamamoto (ELK Corp.) and the hard tissue research team at Kureha Chemical Industry Co., Ltd. for technical assistance. This study was supported by a Grant-in-Aid for Scientific Research from the Japanese Ministry of Education, Culture, Sports, Science, and Technology (15659348).

TABLE 3. EFFECTS OF GONADECTOMIES AND HORMONE REPLACEMENTS ON REPRODUCTIVE TISSUES

	WT			*SRC-1*$^{-/-}$		
	Sham + placebo	*Gonadectomy + placebo*	*Gonadectomy + hormone*	*Sham + placebo*	*Gonadectomy + placebo*	*Gonadectomy + hormone*
Seminal vesicle weights of males (g)	0.31 ± 0.03	0.03 ± 0.01*	0.35 ± 0.03	0.28 ± 0.03	0.03 ± 0.01*	0.18 ± 0.02†
Uterine weights of females (g)	0.12 ± 0.02	0.02 ± 0.01*	0.13 ± 0.03	0.11 ± 0.03	0.02 ± 0.01*	0.05 ± 0.02†

Data are expressed as means ± SEM (n = 8/group for males and females).
*$p < 0.01$, significantly different from the respective sham group.
†$p < 0.01$, significantly different from the respective WT mice.

TABLE 4. COMPARISON BETWEEN TWO *SRC-1*$^{-/-}$ KNOCKOUT MICE

	Modder et al.[29]	*This study*
Generation of mice		
Targeting method	Conventional	Floxed mice × CMV-Cre transgenic mice
Locus of stop codon	Exon 11	Exon 5
Genetic background	C57BL/6	C57BL/6
Physiological conditions		
Age of analysis	12 weeks	12 & 24 weeks
Skeletal phenotype		
12 weeks	Normal	Normal
24 weeks	—	Osteopenia
Hormone administration experiments		
Age	12–20 weeks	16–24 weeks
Estrogen action on females	Decreased	Decreased
Estrogen dose/pellet	15 μg/60-d & 60 μg/60-d	25 μg/60-d
Androgen action on males	—	Decreased
Glucocorticoid action on males	—	Unaffected

REFERENCES

1. Evans RM 1988 The steroid and thyroid hormone receptor superfamily. Science 240:889–895.
2. Mangelsdorf DJ, Thummel C, Beato M, Herrlich P, Schutz G, Umesono K, Blumberg B, Kastner P, Mark M, Chambon P, Evans RM 1995 The nuclear receptor superfamily: The second decade. Cell 83:835–839.
3. Tsai MJ, O'Malley BW 1994 Molecular mechanisms of action of steroid/thyroid receptor superfamily members. Annu Rev Biochem 63:451–486.
4. Bland R 2000 Steroid hormone receptor expression and action in bone. Clin Sci (Lond) 98:217–240.
5. Compston JE 2001 Sex steroids and bone. Physiol Rev 81:419–447.
6. Bilezikian JP 2002 Sex steroids, mice, and men: When androgens and estrogens get very close to each other. J Bone Miner Res 17:563–566.
7. Riggs BL, Khosla S, Melton LJ III 2002 Sex steroids and the construction and conservation of the adult skeleton. Endocr Rev 23:279–302.
8. Francis RM 1999 The effects of testosterone on osteoporosis in men. Clin Endocrinol (Oxf) 50:411–414.
9. Canalis E 1996 Clinical review 83: Mechanisms of glucocorticoid action in bone. Implications to glucocorticoid-induced osteoporosis. J Clin Endocrinol Metab 81:3441–3447.
10. Osella G, Terzolo M, Reimondo G, Piovesan A, Pia A, Termine A, Paccotti P, Angeli A 1997 Serum markers of bone and collagen turnover in patients with Cushing's syndrome and in subjects with adrenal incidentalomas. J Clin Endocrinol Metab 82:3303–3307.
11. Glass CK, Rosenfeld MG 2000 The coregulator exchange in transcriptional functions of nuclear receptors. Genes Dev 14:121–141.
12. McKenna NJ, O'Malley BW 2002 Combinatorial control of gene expression by nuclear receptors and coregulators. Cell 108:465–474.
13. Xu J, O'Malley BW 2002 Molecular mechanisms and cellular biology of the steroid receptor coactivator (SRC) family in steroid receptor function. Rev Endocr Metab Disord 3:185–192.
14. Onate SA, Tsai SY, Tsai MJ, O'Malley BW 1995 Sequence and characterization of a coactivator for the steroid hormone receptor superfamily. Science 270:1354–1357.
15. Hong H, Kohli K, Trivedi A, Johnson DL, Stallcup MR 1996 GRIP1, a novel mouse protein that serves as a transcriptional coactivator in yeast for the hormone binding domains of steroid receptors. Proc Nad Acad Sci USA 93:4948–4952.
16. Voegel JJ, Heine MJ, Zechel C, Chambon P, Gronemeyer H 1996 TIF2, a 160 kDa transcriptional mediator for the ligand-dependent activation function AF-2 of nuclear receptors. EMBO J 15:3667–3675.
17. Carapeti M, Aguiar RC, Watmore AE, Goldman JM, Cross NC 1999 Consistent fusion of MOZ and TIF2 in AML with inv(8)(p11q13). Cancer Genet Cytogenet 113:70–72.
18. Bautista S, Valles H, Walker RL, Anzick S, Zeillinger R, Meltzer P, Theillet C 1998 In breast cancer, amplification of the steroid receptor coactivator gene AIB1 is correlated with estrogen and progesterone receptor positivity. Clin Cancer Res 4:2925–2929.
19. Ghadimi BM, Schrock E, Walker RL, Wangsa D, Jauho A, Meltzer PS, Ried T 1999 Specific chromosomal aberrations and amplification of the AIB1 nuclear receptor coactivator gene in pancreatic carcinomas. Am J Pathol 154:525–536.
20. Xu J, Qiu Y, DeMayo FJ, Tsai SY, Tsai MJ, O'Malley BW 1998 Partial hormone resistance in mice with disruption of the steroid receptor coactivator-1 (SRC-1) gene. Science 279:1922–1925.
21. Weiss RE, Xu J, Ning G, Pohlenz J, O'Malley BW, Refetoff S 1999 Mice deficient in the steroid receptor co-activator 1 (SRC-1) are resistant to thyroid hormone. EMBO J 18:1900–1904.
22. Weiss RE, Gehin M, Xu J, Sadow PM, O'Malley BW, Chambon P, Refetoff S 2002 Thyroid function in mice with compound heterozygous and homozygous disruptions of SRC-1 and TIF-2

coactivators: Evidence for haploinsufficiency. Endocrinology 143: 1554–1557.
23. Takeuchi Y, Murata Y, Sadow P, Hayashi Y, Seo H, Xu J, O'Malley BW, Weiss RE, Refetoff S 2002 Steroid receptor coactivator-1 deficiency causes variable alterations in the modulation of T(3)-regulated transcription of genes in vivo. Endocrinology 143:1346–1352.
24. Nakamichi Y, Shukunami C, Yamada T, Aihara K, Kawano H, Sato T, Nishizaki Y, Yamamoto Y, Shindo M, Yoshimura K, Nakamura T, Takahashi N, Kawaguchi H, Hiraki Y, Kato S 2003 Chondromodulin I is a bone remodeling factor. Mol Cell Biol 23:636–644.
25. Ferretti JL 2000 Peripheral Quantitative Computed Tomography for Evaluating Structural and Mechanical Properties of Small Bone Mechanical Testing of Bone and the Bone-Implant Interface. CRC Press, Boca Raton, FL, USA, pp. 385–405.
26. Parfitt AM, Drezner MK, Glorieux FH, Kanis JA, Malluche H, Meunier PJ, Ott SM, Recker RR 1987 Bone histomorphometry: Standardization of nomenclature, symbols, and units. Report of the ASBMR Histomorphometry Nomenclature Committee. J Bone Miner Res 2:595–610.
27. Heery DM, Kalkhoven E, Hoare S, Parker MG 1997 A signature motif in transcriptional co-activators mediates binding to nuclear receptors. Nature 387:733–736.
28. Spencer TE, Jenster G, Burcin MM, Allis CD, Zhou J, Mizzen CA, McKenna NJ, Onate SA, Tsai SY, Tsai MJ, O'Malley BW 1997 Steroid receptor coactivator-1 is a histone acetyltransferase. Nature 389:194–198.
29. Modder UI, Sanyal A, Kearns AE, Sibonga JD, Nishihara E, Xu J, O'Malley BW, Ritman EL, Riggs BL, Spelsberg TC, Khosla S 2004 Effects of loss of steroid receptor coactivator-1 on the skeletal response to estrogen in mice. Endocrinology 145:913–921.
30. Simpson ER, Mahendroo MS, Means GD, Kilgore MW, Hinshelwood MM, Graham-Lorence S, Amarneh B, Ito Y, Fisher CR, Michael MD, Mendelson CR, Bulun SE 1994 Aromatase cytochrome P450, the enzyme responsible for estrogen biosynthesis. Endocr Rev 15:342–355.
31. Yeh S, Tsai MY, Xu Q, Mu XM, Lardy H, Huang KE, Lin H, Yeh SD, Altuwaijri S, Zhou X, Xing L, Boyce BF, Hung MC, Zhang S, Gan L, Chang C 2002 Generation and characterization of androgen receptor knockout (ARKO) mice: An in vivo model for the study of androgen functions in selective tissues. Proc Natl Acad Sci USA 99:13498–13503.
32. Kawano H, Sato T, Yamada T, Matsumoto T, Sekine K, Watanabe T, Nakamura T, Fukuda T, Yoshimura K, Yoshizawa T, Aihara K, Yamamoto Y, Nakamichi Y, Metzger D, Chambon P, Nakamura K, Kawaguchi H, Kato S 2003 Suppressive function of androgen receptor in bone resorption. Proc Natl Acad Sci USA 100:9416–9421.
33. Vanderschueren D, Van Herck E, De Coster R, Bouillon R 1996 Aromatization of androgens is important for skeletal maintenance of aged male rats. Calcif Tissue Int 59:179–183.
34. Vanderschueren D, van Herck E, Nijs J, Ederveen AG, De Coster R, Bouillon R 1997 Aromatase inhibition impairs skeletal modeling and decreases bone mineral density in growing male rats. Endocrinology 138:2301–2307.
35. Oz OK, Zerwekh JE, Fisher C, Graves K, Nanu L, Millsaps R, Simpson ER 2000 Bone has a sexually dimorphic response to aromatose deficiency. J Bone Miner Res 15:507–514.
36. Morishima A, Grumbach MM, Simpson ER, Fisher C, Qin K 1995 Aromatase deficiency in male and female siblings caused by a novel mutation and the physiological role of estrogens. J Clin Endocrinol Metab 80:3689–3698.
37. Carani C, Qin K, Simoni M, Faustini-Fustini M, Serpente S, Boyd J, Korach KS, Simpson ER 1997 Effect of testosterone and estradiol in a man with aromatase deficiency. N Engl J Med 337:91–95.
38. Smith EP, Boyd J, Frank GR, Takahashi H, Cohen RM, Specker B, Williams TC, Lubahn DB, Korach KS 1994 Estrogen resistance caused by a mutation in the estrogen-receptor gene in a man. N Engl J Med 331:1056–1061.
39. Auger AP, Tetel MJ, McCarthy MM 2000 Steroid receptor coactivator-1 (SRC-1) mediates the development of sex-specific brain morphology and behavior. Proc Natl Acad Sci USA 97: 7551–7555.
40. Bord S, Horner A, Beavan S, Compston J 2001 Estrogen receptors alpha and beta are differentially expressed in developing human bone. J Clin Endocrinol Metab 86:2309–2314.
41. Monroe DG, Johnsen SA, Subramaniam M, Getz BJ, Khosla S, Riggs BL, Spelsberg TC 2003 Mutual antagonism of estrogen receptors alpha and beta and their preferred interactions with steroid receptor coactivators in human osteoblastic cell lines. J Endocrinol 176:349–357.
42. Picard F, Gehin M, Annicotte J, Rocchi S, Champy MF, O'Malley BW, Chambon P, Auwerx J 2002 SRC-1 and TIF2 control energy balance between white and brown adipose tissues. Cell 111:931–941.
43. Takeda S, Karsenty G 2001 Central control of bone formation. J Bone Miner Metab 19:195–198.
44. Yanagisawa J, Kitagawa H, Yanagida M, Wada O, Ogawa S, Nakagomi M, Oishi H, Yamamoto Y, Nagasawa H, McMahon SB, Cole MD, Tora L, Takahashi N, Kato S 2002 Nuclear receptor function requires a TFTC-type histone acetyl transferase complex. Mol Cell 9:553–562.
45. Liu YZ, Liu YJ, Recker RR, Deng HW 2003 Molecular studies of identification of genes for osteoporosis: The 2002 update. J Endocrinol 177:147–196.
46. Adachi M, Takayanagi R, Tomura A, Imasaki K, Kato S, Goto K, Yanase T, Ikuyama S, Nawata H 2000 Androgen-insensitivity syndrome as a possible coactivator disease. N Engl J Med 343: 856–862.

Address reprint requests to:
Hiroshi Kawaguchi, MD, PhD
Department of Orthopaedic Surgery
Faculty of Medicine
University of Tokyo
Hongo 7-3-1, Bunkyo
Tokyo 113-8655, Japan
E-mail: kawaguchi-ort@h.u-tokyo.ac.jp

Received in original form December 19, 2003; in revised form April 14, 2004; accepted May 7, 2004.

THE JOURNAL OF BIOLOGICAL CHEMISTRY

Vol. 279, No. 32, Issue of August 6, pp. 33684–33695, 2004
Printed in U.S.A.

Reduced Pain Hypersensitivity and Inflammation in Mice Lacking Microsomal Prostaglandin E Synthase-1*

Received for publication, January 8, 2004, and in revised form, April 22, 2004
Published, JBC Papers in Press, May 12, 2004, DOI 10.1074/jbc.M400199200

Daisuke Kamei‡§, Kiyofumi Yamakawa§¶, Yui Takegoshi‡, Maya Mikami-Nakanishi‡, Yoshihito Nakatani‡, Sachiko Oh-ishi‡, Hidekazu Yasui‖, Yoshiaki Azuma‖, Noriyasu Hirasawa, Kazuo Ohuchi**, Hiroshi Kawaguchi¶, Yukio Ishikawa‡‡, Toshiharu Ishii‡‡, Satoshi Uematsu§§, Shizuo Akira§§, Makoto Murakami‡, and Ichiro Kudo‡¶¶**

*From the ‡Department of Health Chemistry, School of Pharmaceutical Sciences, Showa University, 1-5-8 Hatanodai, Shinagawa-ku, Tokyo 142-8555, the ¶Department of Orthopedic Surgery, Faculty of Medicine, University of Tokyo, 7-3-1 Hongo, Bunkyo-ku, Tokyo 113-8655, ‖Pharmaceutical Discovery Research Laboratories, the Institute for Biomedical Researh, Teijin Pharma Limited, 4-3-2 Asahigaoka, Hino-shi, Tokyo 191-8512, the **Laboratory of Pathophysiological Biochemistry, Graduate School of Pharmaceutical Sciences, Tohoku University, Aoba Aramaki, Aoba-ku, Sendai, Miyagi 980-8578, the ‡‡Department of Pathology, Toho University, School of Medicine, 5-21-16 Omori-Nishi, Ohta-ku, Tokyo 143-8540, and the §§Department of Host Defense, Research Institute for Microbial Diseases, Osaka University, 3-1 Yamada-oka, Suita, Osaka 565-0871, Japan*

We examined the *in vivo* role of membrane-bound prostaglandin E synthase (mPGES)-1, a terminal enzyme in the PGE_2-biosynthetic pathway, using mPGES-1 knockout (KO) mice. Comparison of PGES activity in the membrane fraction of tissues from mPGES-1 KO and wild-type (WT) mice indicated that mPGES-1 accounted for the majority of lipopolysaccharide (LPS)-inducible PGES in WT mice. LPS-stimulated production of PGE_2, but not other PGs, was impaired markedly in mPGES-1-null macrophages, although a low level of cyclooxygenase-2-dependent PGE_2 production still remained. Pain nociception, as assessed by the acetic acid writhing response, was reduced significantly in KO mice relative to WT mice. This phenotype was particularly evident when these mice were primed with LPS, where the stretching behavior and the peritoneal PGE_2 level of KO mice were far less than those of WT mice. Formation of inflammatory granulation tissue and attendant angiogenesis in the dorsum induced by subcutaneous implantation of a cotton thread were reduced significantly in KO mice compared with WT mice. Moreover, collagen antibody-induced arthritis, a model for human rheumatoid arthritis, was milder in KO mice than in WT mice. Collectively, our present results provide unequivocal evidence that mPGES-1 contributes to the formation of PGE_2 involved in pain hypersensitivity and inflammation.

Prostaglandin (PG)[1] E_2 is the most common prostanoid, being produced by a variety of cells and tissues, and has a broad range of biological activity. Recent advances in this research field have led to molecular identification and characterization of various enzymes involved in the biosynthesis of PGE_2, including phospholipase A_2 (PLA_2), cyclooxygenase (COX) and terminal PGE synthase (PGES) (1). Each of these three enzymatic steps can be rate limiting for PGE_2 biosynthesis and involves multiple enzymes/isozymes that can act in different phases of cell activation. The PGE_2 produced thus far is then released from the cells and acts on the four types of PGE receptor, EP1, EP2, EP3, and EP4, which are coupled with trimeric G protein signaling (2).

PGES, which catalyzes the conversion of PGH_2 to PGE_2, exists as membrane-associated and cytosolic enzymes. Two of them are membrane-bound enzymes and have been designated as mPGES-1 and mPGES-2 (3–16). mPGES-1 is a glutathione (GSH)-requiring perinuclear protein belonging to the MAPEG (for membrane-associated proteins involved in eicosanoid and GSH metabolism) family (4–6). This enzyme is induced markedly by proinflammatory stimuli, is down-regulated by anti-inflammatory glucocorticoids, and is functionally coupled with COX-2 in marked preference to COX-1. Induction of mPGES-1 expression has also been observed in various systems in which COX-2-derived PGE_2 has been implicated to play a critical role, such as inflammation, fever, pain, female reproduction, tissue repair, and cancer (4–12). Inducible expression of mPGES-1 is in part regulated by the mitogen-activated protein kinase pathways (13), where the kinases may switch on the inducible transcription factor Egr-1 that in turn binds to the proximal GC box in the *mPGES-1* promoter, leading to mPGES-1 transcription (14). mPGES-2, which has a catalytic glutaredoxin- or thioredoxin-like domain and is activated by various thiol reagents, is synthesized as a Golgi membrane-associated protein, and the proteolytic removal of the N-terminal hydrophobic domain leads to the formation of a mature cytosolic enzyme (15, 16). This enzyme is rather constitutively expressed in various cells and tissues and is functionally coupled with both COX-1 and COX-2 (16). Cytosolic PGES (cPGES), a GSH-requiring enzyme constitutively expressed in a wide variety of cells, is functionally linked to COX-1, not COX-2, to promote immediate PGE_2 production (17). This enzyme is regulated by formation of a complex with Hsp90, a molecular chaperone (18). In addition, two cytosolic GSH-*S*-transferases (μ2 and μ3) have the ability to catalyze the isomerization of PGH_2 to PGE_2, at least *in vitro* (19).

* This work was supported by grants-in aid for scientific research from the Ministry of Education, Science, Culture, Sports, and Technology of Japan. The costs of publication of this article were defrayed in part by the payment of page charges. This article must therefore be hereby marked "*advertisement*" in accordance with 18 U.S.C. Section 1734 solely to indicate this fact.

§ These authors equally contributed to this work.

¶¶ To whom correspondence should be addressed. Tel.: 81-3-3784-8196; Fax: 81-3-3784-8245; E-mail: kudo@pharm.showa-u.ac.jp.

[1] The abbreviations used are: PG, prostaglandin; BMD, bone mineral density; CAIA, collagen antibody-induced arthritis; CIA, collagen-induced arthritis; COX, cyclooxygenase; cPGES, cytosolic PGES; $cPLA_2\alpha$, cytosolic phospholipase $A_2\alpha$; HDC, histidine decarboxylase; KO, knockout; LPS, lipopolysaccharide; mPGES, membrane-bound PGES; PGES, PGE synthase; siRNA, small interfering RNA; TBS, Tris-buffered saline; TRAP, tartrate-resistant acid phosphatase; VEGF, vascular endothelial cell growth factor; WT, wild-type.

The importance of PGE_2 in various pathophysiological events dictates the necessity to understand the role of each PGES enzyme *in vivo*. In fact, biochemical and cell biological analyses have led to the proposal that among the PGES enzymes identified so far, mPGES-1 may be most critically responsible for the production of the PGE_2 implicated in various pathophysiological events. An initial study with mPGES-1 knock-out (KO) mice has reported the essential role of mPGES-1 in lipopolysaccharide (LPS)-stimulated delayed PGE_2 production by macrophages, although these mice are fertile, develop normally after birth, and retain LPS-stimulated production of various cytokines (20). In this study, we used mPGES-1 KO mice to analyze the role of mPGES-1 in inflammation-associated pain hypersensitivity, tissue granulation accompanying angiogenesis, and arthritis induced by collagen antibody.

EXPERIMENTAL PROCEDURES

Animals—Male C57BL/6 mice were obtained from Saitama Animal Center. The mPGES-1 KO mice and littermate wild-type (WT) mice (C57BL/6 × 129/SvJ background) were described previously (20). Male mice (7 weeks old) were used in each experiment. Mice were housed in microisolator cages in a pathogen-free barrier facility, and all experiments were performed under approved institutional guidance.

Agents—LPS (*Escherichia coli* 0111:B4), goat anti-mouse vascular endothelial cell growth factor (VEGF), and indomethacin were purchased from Sigma. Mouse anti-human $cPLA_2\alpha$ monoclonal antibody and goat anti-human COX-1 and COX-2 polyclonal antibodies were purchased from Santa Cruz Biotechnology. Rabbit antibodies against human mPGES-1 (12), mPGES-2 (16), and cPGES (17) were prepared as described previously. Rabbit anti-mouse histidine decarboxylase (HDC) antibody was donated by Dr. S. Tanaka (Kyoto University) (21). Enzyme immunoassay kits for PGE_2, 6-keto-$PGF_{1\alpha}$ (a stable end product of PGI_2), $PGF_{2\alpha}$, and thromboxane B_2 (a stable end product of thromboxane A_2) and the COX-2 inhibitor NS-398 were purchased from Cayman Chemicals. The COX-1 inhibitor valeryl salicylate was a generous gift from Dr. W. Smith (University of Michigan). Oligonucleotides were purchased from Bex.

Measurement of PGES Activity—PGES activity was measured by assessment of conversion of PGH_2 to PGE_2 as reported previously (4). Briefly, cell or tissue homogenates were centrifuged at 100,000 × *g* for 1 h at 4 °C, and the membrane fractions were used as an enzyme source. An aliquot (10 μg of protein equivalents) was incubated with 0.5 μg of PGH_2 for 30 s at 24 °C in 0.1 ml of 0.1 M Tris-HCl (pH 8.0) containing 1 mM glutathione and 5 μg of indomethacin. After stopping the reaction by the addition of 100 mM $FeCl_2$, the PGE_2 content of the reaction mixture was quantified by use of the enzyme immunoassay kit.

Preparation and Activation of Peritoneal Macrophages—Peritoneal cells were recovered from mice that had received thioglycollate medium (Difco) (1 ml/20 g of body weight) 4 days before (22). The peritoneal cells were seeded into 6- or 12-well plates (Iwaki Glass) at a cell density of 10^6 cells/ml in 2 ml (for 6-well plates) or 1 ml (for 12-well plates) of RPMI medium (Nissui) supplemented with 10% (v/v) fetal calf serum. After incubation for 2 h in a CO_2 incubator, the supernatants and nonadherent cells were removed. More than 90% of adherent cells were macrophages. Then the cells were incubated with or without 10 μg/ml LPS in medium containing 2% serum for appropriate periods. The supernatants were taken for enzyme immunoassay for prostanoids, and the cells were subjected to Western blotting (see below).

Experiments with mPGES-1 Small Interfering RNA (siRNA)—Two synthetic hairpin-forming oligonucleotides directed at mPGES-1, 5′-GATCCCGGCCTTTGCCAACCCCGAGTTCAAGAGACTCGGGGTTGGCAAAGGCCTTTTTTGGAAA-3′ (sense) and 3′-AGCTTTTCCAAAAAAGGCCTTTGCCAACCCCGAGTCTCTTGAACTCGGGGTTGGCAAAGGCCGG-5′ (antisense), both of which harbored BamHI and HindIII sites at their 5′- and 3′-ends, respectively, were annealed, cut with BamHI and XbaI, and then ligated into the BamHI/XbaI-digested pRNA-U6.1/Hygro vector (GenScript) using T4 ligase (Takara Biomedicals). After transformation into DH5α-competent cells (TOYOBO), the plasmid was extracted and purified using the Endofree Plasmid Maxi Kit (Qiagen).

Transfection of the plasmid into peritoneal macrophages was performed by lipofection, as described previously (4). Briefly, 5 μg of the plasmid was mixed with 10 μl of LipofectAMINE 2000 (Invitrogen) in 100 μl of Opti-MEM (Invitrogen) for 30 min and then added to macrophages in 0.5 ml of Opti-MEM in 12-well plates. After incubation for 24 h, the medium was replaced with 1 ml of fresh culture medium and then incubated with or without 10 μg/ml LPS in medium containing 2% fetal calf serum for 16 h.

Acetic Acid Writhing Reaction—The writhing reaction was induced in mice by intraperitoneal injection of 0.9% (v/v) acetic acid solution at a dose of 5 ml/kg, as described previously (23, 24). In one group of animals, LPS (10 μg/0.1 ml of saline/mouse) was given intraperitoneally 18 h before the injection of acetic acid solution. A suspension of 1 mg/ml indomethacin in 1% (w/v) sodium carboxymethylcellulose solution was injected subcutaneously into mice (at final dose of 10 mg/kg indomethacin/mouse) 30 min before the injection of acetic acid solution. The number of writhing responses was counted every 5 min.

For measurement of prostanoids, mice were sacrificed 15 min after acetic acid injection, and their peritoneal cavities were washed twice with Hanks' balanced salt solution (Nissui) containing 10 μM indomethacin. The pooled peritoneal fluids were adjusted to pH 3.0 with 1 N HCl and passed through Sep-Pak C18 cartridges (Waters), and the retained PGs were eluted from the cartridges with 8 ml of methanol, as described previously (23, 24). A trace amount of [^{3}H]PGE_2 (Cayman Chemicals) was added to the samples before passage through the cartridges to calibrate the recovery of PGs. The solvent of the samples was evaporated, and then PGs were dissolved in an aliquot of buffer and assayed with commercial enzyme immunoassay kits for each PG.

Cotton Thread-induced Granulation Tissue Formation—Cotton threads (Araiwa Co.) were washed overnight with ethyl acetate and dried at room temperature before being cut into 1-cm lengths (3 mg weight), and sterilized by dry heat at 180 °C for 2 h. The cotton threads were implanted subcutaneously into the dorsum of anesthetized mice by using a 13-gauge implant needle (Natume), as described previously (25). After appropriate periods, the mice were anesthetized and killed, and the granulation tissues were dissected together with the cotton threads and weighed. As required for the experiments, indomethacin (5 mg/kg) or vehicle was injected intraperitoneally every day. The isolated granulation tissues were washed, cut into small pieces with scissors, and homogenized with a Polytron homogenizer in a homogenizing buffer comprising 20 mM Tris-HCl (pH 7.4), 250 mM sucrose, 0.5 mM EDTA, 10 μM indomethacin, 1 μM phenylmethylsulfonyl fluoride, and 0.5% (v/v) Triton X-100. The obtained tissue homogenates were centrifuged at 3,000 rpm for 5 min, and 200-μl aliquots of the supernatants were centrifuged again at 14,000 × *g* for 30 min at 4 °C. Then, the hemoglobin concentrations in the supernatants were determined spectrophotometrically by measuring the absorbance at 540 nm with a hemoglobin assay kit (Wako). PGs were extracted from the homogenates with Sep-Pak C18 cartridges and quantified by enzyme immunoassay, as described above.

Western Blotting—Aliquots of samples (20-μg protein equivalents) were subjected to SDS-PAGE using 7.5% (for $cPLA_2\alpha$ and COXs) or 12.5% (for PGESs) gels under reducing conditions. The separated proteins were electroblotted onto nitrocellulose membranes (Schleicher & Schuell) with a semidry blotter (MilliBlot-SDE system; Millipore). After blocking with 3% (w/v) skim milk in Tris-buffered saline (TBS (pH 7.4)) containing 0.05% Tween 20 (TBS-Tween), the membranes were probed with the respective antibodies (1:5,000 dilution for $cPLA_2\alpha$, COX-2, and PGESs; 1:1,000 dilution for VEGF; 1:2,500 dilution for HDC, and 1:20,000 dilution for COX-1 in TBS-Tween) for 2 h, followed by incubation with horseradish peroxidase-conjugated anti-mouse (for $cPLA_2\alpha$), anti-rabbit (for PGESs and HDC), or anti-goat (for COXs and VEGF) IgG antibody (1:5,000 dilution in TBS-Tween) for 2 h, and were visualized with the ECL Western blot system (PerkinElmer Life Sciences), as described previously (4).

Immunohistochemistry—Formalin-fixed, paraffin- embedded sections of the granulation tissue sections were incubated with Target Retrieval Solution (DAKO) as required, incubated for 10 min with 3% (v/v) H_2O_2, washed three times with TBS for 5 min each, incubated for 30 min with 5% (v/v) skim milk, washed three times with TBS-Tween for 5 min each, and incubated for 2 h with anti-mPGES-1 antibody in TBS (1:100 dilution). After five washes, the sections were treated with the CSA system staining kit (DAKO) followed by counterstaining with hematoxylin and eosin, as described previously (12).

Arthritis Model—Arthritis was induced in mPGES-1 KO and WT mice by the modified method of Terato *et al.* (26, 27). Briefly, mice were injected intraperitoneally with 10 mg of anti-type II collagen monoclonal antibodies (Immuno-Biological Laboratory) on day 0. On days 2 and 7, 50 μg of LPS (100 μl of 500 μg/ml solution in saline) was injected intraperitoneally followed by an intermittent LPS injection every 3 days to the end of the experiments. As a control, 2.5 or 0.1 ml of saline was injected in place of the antibodies or LPS, respectively. The clinical

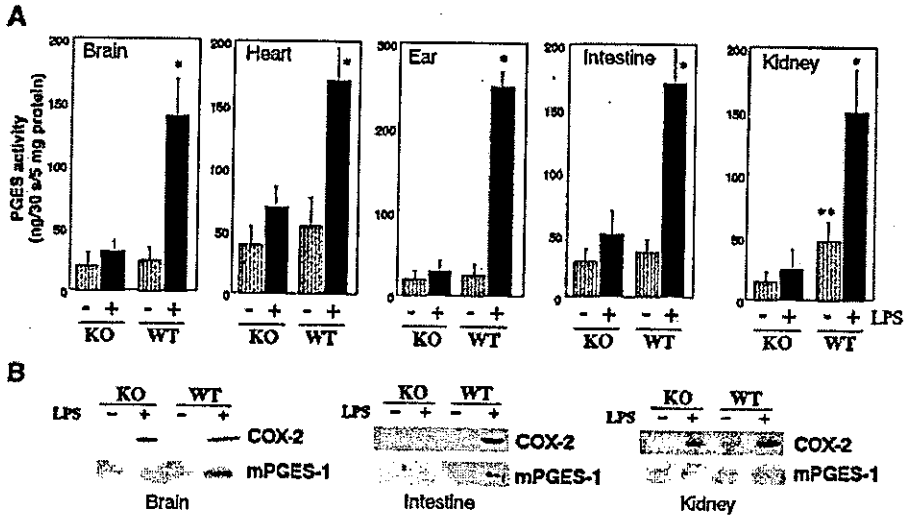

FIG. 1. **PGES enzymatic activities in tissues of WT and mPGES-1 KO mice.** *A*, tissues from WT and mPGES-1 KO mice treated for 24 h with (+) or without (−) LPS were homogenized, and PGES enzymatic activities in their membrane fractions were assessed. *, $p < 0.05$ *versus* each LPS-untreated group of WT mice; **, $p < 0.05$ *versus* LPS-untreated kidney of KO mice ($n = 3–4$). *B*, expression of mPGES-1 in several tissues of WT and KO mice with or without LPS treatment as assessed by Western blotting. Representative results of three or four independent experiments are shown.

severity of arthritis was graded on a 0–3 scale as follows: 0, normal; 1, swelling of ankle or wrist, or limited to digits; 2, swelling of the entire paw; 3, maximal swelling. Each limb was graded by a single blinded observer, allowing a maximum arthritis score of 12 for each animal. On day 28, the mice were anesthetized with ketamine/xylazine solution and a radiograph was taken with a soft x-ray apparatus (CMB-2; SOFTEX). After perfusion of mice with 4% (w/v) buffered paraformaldehyde, fore and right hind limbs were removed, decalcified in 10% (w/v) EDTA, and embedded in paraffin, and 5-μm sections were stained with hematoxylin and eosin or toluidine blue. Bone resorption was evaluated by the tartrate-resistant acid phosphatase (TRAP) staining of the carpometacarpal joints. TRAP-positive cells were stained at pH 5.0 in the presence of L(+)-tartaric acid using naphthol AS-MX phosphate (Sigma) in *N,N*-dimethylformamide as the substrate. The specimens were subjected to histomorphometric analyses using a semiautomated system (Osteoplan II; Carl Zeiss), and measurements were made at a magnification of ×400. Osteoclast number and eroded surface were measured at the carpometacarpal joints in the metacarpal bones.

After perfusion fixation, left femora and tibiae were excised and bone mineral density (BMD) was measured by dual energy x-ray absorptiometry using a bone mineral analyzer (DCS-600; Aloka Co.). To evaluate bone destruction of the knee joint area, BMDs of four equal longitudinal divisions in femur and tibia were measured, and the BMD around the knee joint was expressed by the sum of those in the distal one-fourth of femur and in the proximal one-fourth of tibia (28).

On day 6, all four paws including wrist or ankle joints were collected and homogenized in a homogenizing buffer. Then, aliquots were taken for PGE_2 enzyme immunoassay and Western blotting, as described above.

Other Methods—Protein concentrations were determined by a bicinchoninic acid protein assay kit (Pierce) with bovine serum albumin (Sigma) as a standard. Data were analyzed by Student's *t* test. Results are expressed as the mean ± S.E., with $p = 0.05$ as the limit of significance.

RESULTS

mPGES-1 Is a Major Inducible PGES in Vivo—Fig. 1*A* illustrates PGES enzymatic activities in the membrane fraction of various tissues from mPGES-1 KO and WT mice with or without 24-h treatment with LPS. Basal PGES activities (*i.e.* without LPS administration) in the brain, heart, intestine, and ear were similar between WT and KO mice, whereas the activity in the kidney of WT mice was about 4-fold higher than that of KO mice (Fig. 1*A*). Treatment of WT mice with LPS resulted in 3–8-fold increases in PGES activity over the basal levels of the individual tissues. In tissues of mPGES-1 KO mice, LPS-stimulated increases in PGES activity over the basal levels were only modest, although <2-fold increases were consistently observed in all tissues examined (Fig. 1*A*).

Immunoblotting of the membrane fractions of individual tissues revealed that the expression of mPGES-1 was markedly induced in tissues of WT mice, whereas no mPGES-1 protein was detected in tissues of KO mice (Fig. 1*B*). Constitutive expression of mPGES-1 was seen only in the kidney of WT mice (Fig. 1*B*), in agreement with a recent immunohistochemical study demonstrating the expression of mPGES-1 in the epithelia of distal tubules and medullary collecting ducts in this organ (29). In the brain (Fig. 1*B*), heart, and ear (data not shown), LPS-induced COX-2 expression in KO mice was similar to that in WT mice. In the intestine and kidney, COX-2 expression in LPS-treated KO mice was significantly lower than that in replicate WT mice (Fig. 1*B*), suggesting that mPGES-1-derived PGE_2 amplifies COX-2 induction in these tissues. Thus, mPGES-1 represents a major inducible membrane-associated PGES in various tissues of LPS-treated mice. However, the fact that substantial levels of PGES activity still exist in tissues of KO mice implies the presence of another membrane-bound PGES that is expressed rather constitutively.

Evaluation of the Role of mPGES-1 in PGE_2 Production by LPS-stimulated Macrophages—Accumulating evidence suggests that delayed PGE_2 production by LPS-stimulated macrophages depends on inducible COX-2 and mPGES-1 (4, 20, 22). To reevaluate the contribution of mPGES-1 to this event, we first took advantage of siRNA technology. As shown in Fig. 2*A*, *ex vivo* stimulation of C57BL/6 mouse-derived thioglycollate-induced peritoneal macrophages with LPS led to a marked increase in PGE_2 production, which was accompanied by *de novo* induction of COX-2 and mPGES-1. This PGE_2-biosynthetic response was reduced dramatically in replicate cells transfected with mPGES-1 siRNA, in which mPGES-1 expression was greatly decreased without reduction of COX-2 expression (Fig. 2*A*). This indicates that mPGES-1 contributes to the production of the majority of PGE_2 in LPS-stimulated macrophages.

Consistent with this observation, LPS-stimulated PGE_2 production was impaired markedly in macrophages derived from mPGES-1 KO mice relative to those derived from WT mice over the entire culture period (Fig. 2*B*). Constitutive expression of

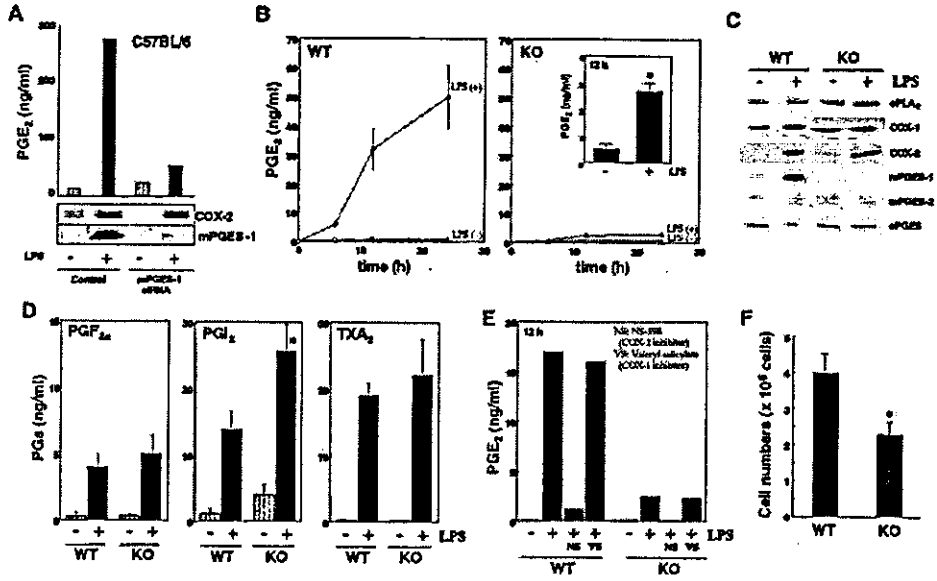

FIG. 2. **mPGES-1 is an essential component for PGE_2 production by LPS-stimulated macrophages.** *A*, peritoneal macrophages derived from C57BL/6 mice were transfected with mPGES-1 siRNA or mock control and then treated for 24 h with (+) or without (−) LPS. PGE_2 released into the supernatants was quantified. Cells were subjected to Western blotting for COX-2 and mPGES-1 (*bottom*). *B*, peritoneal macrophages obtained from WT and mPGES-1 KO mice were incubated for the indicated periods with or without LPS to assess PGE_2 release. PGE_2 production by KO macrophages is magnified in the *inset*. *C*, Western blotting of the PGE_2 biosynthetic enzymes in WT- and KO-derived macrophages after 24-h culture with (+) or without (−) LPS. *D*, production of other PGs by WT and KO macrophages after 24-h culture with (+) or without (−) LPS. *E*, effects of COX isozyme-selective inhibitors on LPS-stimulated PGE_2 production by WT and KO macrophages. *F*, numbers of macrophages recovered from the peritoneal cavities of thioglycollate-treated WT and KO mice. In *B*, *D*, and *F*, values are the mean ± S.E. of four independent experiments. A representative result of two reproducible experiments is shown in *A*, *C*, and *E*.

$cPLA_2\alpha$, COX-1, cPGES, and mPGES-2 (appearing as a doublet, reflecting the processed and unprocessed forms (16)) and inducible expression of COX-2 were similar between WT- and KO-derived macrophages (Fig. 2*C*), indicating that mPGES-1 deficiency does not affect the expression of other enzymes implicated in PGE_2 synthesis in these cells. The levels of other prostanoids, including $PGF_{2\alpha}$, thromboxane A_2, and particularly PGI_2, produced by mPGES-1 KO cells were modestly higher than those produced by WT cells (Fig. 2*D*), which may reflect a shunting effect because of the defect of the metabolic flow from PGH_2 to PGE_2.

It should be noted, however, that a small but significant production of PGE_2 was still observed in mPGES-1-deficient macrophages (Fig. 2*B*). The level of PGE_2 released by mPGES-1-null macrophages reached as much as 8% of that produced by WT cells after 12-h culture with LPS (Fig. 2*B*, *inset*). To assess which COX isoforms contribute to PGE_2 production in mPGES-1-deficient macrophages, the effects of specific inhibitors of COX-1 (valeryl salicylate) and COX-2 (NS-398) on PGE_2 generation were examined. As shown in Fig. 2*E*, PGE_2 production was reduced markedly by NS-398, whereas valeryl salicylate was without effect in both WT and KO cells. This result indicates that the small production of PGE_2 observed in mPGES-1-null macrophages still depends largely on COX-2. Because mPGES-2 and cPGES were expressed in these cells (Fig. 2*C*), this small PGE_2 production might occur through these enzymes.

During the course of this study, we noted that the number of macrophages recovered from the peritoneal cavity 4 days after the injection of thioglycollate was significantly lower in mPGES-1 KO mice than in WT mice (Fig. 2*F*). This result suggests that mPGES-1-derived PGE_2 may participate in the migration of macrophages into inflamed sites, an event also found in the model of inflammatory granulation tissue formation (see below).

Participation of mPGES-1 in Pain Nociception—During the inflammatory reaction, pain is produced through complex interactions between various inflammatory mediators, one of which is PGE_2. Studies using COX inhibitors as well as PG receptor-deficient mice have established the important role of PGE_2 as well as PGI_2 in pain nociception (24, 30–32). We therefore used the acetic acid writhing test to evaluate the contribution of mPGES-1 to the production of PGE_2 involved in nociceptive pain perception. We were particularly interested in inflammatory pain hypersensitivity in LPS-pretreated animals because the expression levels of both COX-2 and mPGES-1 are markedly elevated after LPS treatment (Figs. 1 and 2).

Injection of acetic acid into the peritoneum of WT mice induced stretching behavior, which peaked at 5–10 min and then declined gradually over 30 min (Fig. 3*A*, *upper panel*). This basal writhing response was augmented significantly at all time points if LPS had been injected into mice 24 h before acetic acid injection (Fig. 3*A*, *lower panel*). Notably, the LPS-primed, acetate-induced pain response was reduced markedly in mPGES-1 KO mice compared with that in replicate WT mice over the entire experimental period (Fig. 3*B*, *lower panel*). Under LPS-unprimed (basal) conditions, the writhing response of mPGES-1 KO mice was also significantly less than that of WT mice (Fig. 3*B*, *upper panel*), although the difference between WT and KO mice was less obvious than that observed after LPS priming. Thus, the total numbers of stretching of mPGES-1 KO mice over the initial 15 min after acetic acid administration were reduced by ~45 and ~80% relative to those of WT mice under basal and LPS-primed conditions, respectively (Table I). Both the basal and LPS-primed writhing responses of WT mice were reduced by 70–80% by treatment with indomethacin (Fig. 3*C*). These results collectively suggest that mPGES-1-derived PGE_2 is a main mediator of LPS-primed pain hypersensitivity, whereas the basal pain response may also involve PGE_2 produced by other PGES(s) or other additional prostanoid(s) such as PGI_2, because this pain response is reduced markedly in mice lacking the PGI receptor IP (24, 30).

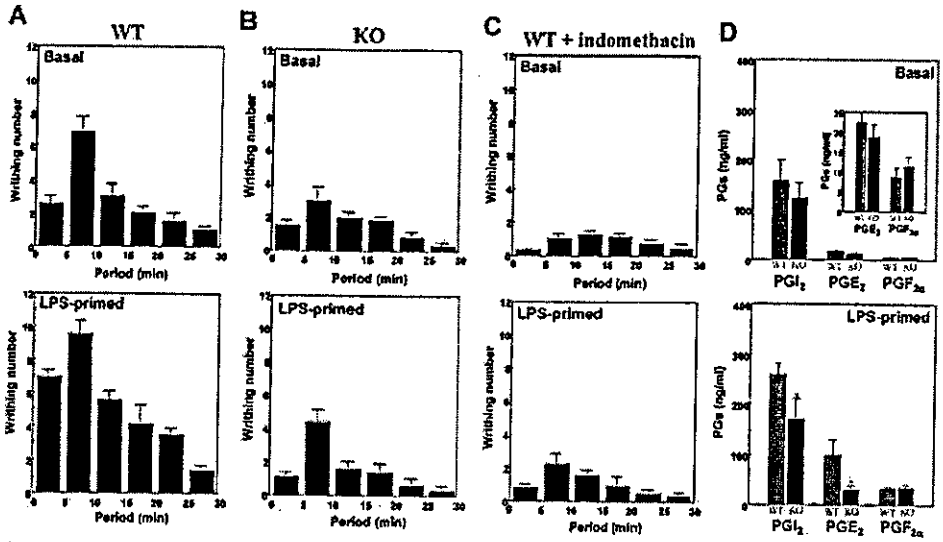

FIG. 3. **Impaired pain hypersensitivity in mPGES-1-deficient mice.** *A–C*, the acetic acid writhing reaction of WT (*A* and *C*) and mPGES-1 KO (*B*) mice before (*upper*) and 24 h after (*lower*) treatment with LPS. In *C*, indomethacin was administered to WT mice 2 h before acetic acid challenge. Values are the mean ± S.E. (n = 12–13; *, $p < 0.05$). *D*, levels of prostanoids in the peritoneal cavities of LPS-primed (*lower*) and unprimed (*upper*) mice 15 min after injection of acetic acid. Levels of PGE_2 and $PGF_{2\alpha}$ in LPS-unprimed mice are magnified in the *inset*. Values are the mean ± S.E. (n = 7; *, $p < 0.05$).

TABLE I
Reduced pain response in mPGES-1 KO mice

The total numbers of writhing reaction over the initial 15 min after the acetic acid administration are shown. Values are the mean ± S.E. (n = 12–13). *, $p < 0.05$ *versus* WT without LPS priming; **, $p < 0.05$ *versus* respective WT control. IM, indomethacin.

Mice	LPS priming	Writhing numbers
WT	−	10.3 ± 0.9
WT	+	20.1 ± 2.4 *
KO	−	5.5 ± 0.6**
KO	+	7.1 ± 0.6**
WT + IM	−	3.0 ± 0.8**
WT + IM	+	4.5 ± 0.6**

In WT mice, the level of PGE_2 in the peritoneal cavity 15 min after acetic acid injection was about 6-fold higher in the LPS-primed group than in the LPS-unprimed group (Fig. 3*D*), in agreement with the elevated expression of COX-2 and mPGES-1 in response to LPS (see Figs. 1 and 2). In mPGES-1 KO mice, peritoneal PGE_2 levels were reduced only by ~15% (this difference was statistically insignificant) and by as much as ~70% compared with those in WT mice under the basal and LPS-primed conditions, respectively (Fig. 3*D*). Given that the reduction of the peritoneal PGE_2 level is less marked than that of the writhing response in KO mice, particularly under LPS-unprimed condition, we speculate that PGE_2 produced in the spinal cord and dorsal root ganglia, in which a trace level of mPGES-1 is constitutively expressed (33), might also affect pain perception by spinal neurons. As reported previously (23, 24), PGI_2 is the major prostanoid released into the peritoneal cavities of mice during the acetic acid writhing response with or without LPS priming (Fig. 3*D*). Consistent with the elevation of COX-2 expression after LPS treatment, the peritoneal PGI_2 level was 1.8-fold higher in LPS-treated than in untreated WT mice (Fig. 3*D*). Interestingly, the levels of PGI_2 in mPGES-1 KO mice were significantly lower than in WT mice after LPS priming (Fig. 3*D*), suggesting partial dependence of PGI_2 synthesis on mPGES-1-derived PGE_2 in this setting. Production of $PGF_{2\alpha}$ was increased 3-fold after LPS priming and was unaffected by mPGES-1 deficiency in both basal and LPS-primed situations (Fig. 3*D*). The greater -fold increase in $PGF_{2\alpha}$ than in PGI_2 after LPS treatment may reflect distinct functional coupling between COX-2 and various terminal synthases (34) or LPS-mediated induction of $PGF_{2\alpha}$ synthase (35). Indomethacin treatment of WT mice reduced the peritoneal PGI_2 levels by >90% with or without LPS priming (data not shown), indicating that the reduced writhing response by indomethacin (Fig. 3*C*) is related to almost complete inhibition of COX enzymes.

Participation of mPGES-1 in Inflammatory Granulation and Angiogenesis—Subcutaneous implantation of a cotton thread in the dorsum of mice induces formation of granulation tissue with angiogenesis (25). As shown in Fig. 4*A*, granulation tissue formation and angiogenesis around the implanted cotton thread were obvious in C57BL/6 mice, events that were ameliorated in replicate mice treated with indomethacin, implying the involvement of prostanoid(s). Quantification studies revealed that the weights of and the levels of hemoglobin (an indicator of angiogenesis) and PGE_2 in the granulation tissue were reduced significantly in indomethacin-treated mice compared with vehicle-treated mice (Fig. 4*B*).

To evaluate the contribution of mPGES-1 to this inflammatory process, cotton threads were implanted into the dorsum tissues of mPGES-1 WT and KO mice. As in the case of C57BL/6 mice, progressive formation of granulation tissue and vascular networks in the subcutaneous tissues around the implanted cotton thread was visually obvious in WT mice, and this process peaked on day 5 (Fig. 4*C*). In comparison, formation of granulation tissue and blood vessels appeared mild in mPGES-1-deficient mice (Fig. 4*C*). Accordingly, there was a significant increase in the wet weight of the cotton thread-associated granulation tissue in WT mice over days 5–7, whereas this increase was not observed appreciably in mPGES-1 KO mice (Fig. 4*D*, *left panel*). Angiogenesis, as quantified by hemoglobin levels, in the granulation tissue peaked on days 3–5 in WT mice and then declined, and there was ~50% reduction in hemoglobin levels in KO mice relative to WT mice (Fig. 4*D*, *middle panel*). PGE_2 levels in the granulation tissue of WT mice peaked on days 1–3 and then declined (Fig. 4*D*, *right panel*). Thus, it appears that increased PGE_2 production kinetically precedes angiogenesis, followed by granulation tissue formation in WT mice. In mPGES-1 KO mice, PGE_2 levels were almost constant throughout the experimental period, and

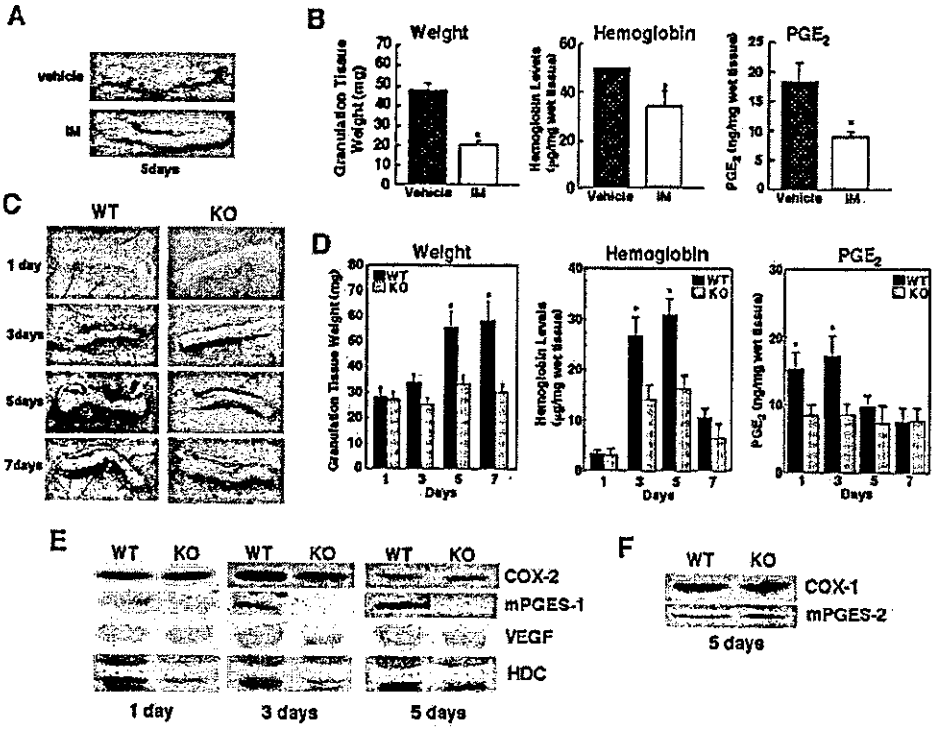

FIG. 4. **Reduced inflammatory granulation tissue formation and angiogenesis in mPGES-1 KO mice.** *A* and *B*, a cotton thread was implanted subcutaneously in the dorsum of C57BL/6 mice with or without indomethacin (*IM*) treatment. After taking photographs on day 5 (*A*), changes in wet weights of, and hemoglobin and PGE_2 levels in, the isolated granulation tissues were quantified (*B*). Values are the mean ± S.E. ($n = 7$; *, $p < 0.05$ *versus* replicate WT mice). *C–F*, a cotton thread was implanted subcutaneously in the dorsum of WT and mPGES-1 KO mice. Photographs indicate granulation tissues and vascular networks around the cotton thread on days 1, 3, 5, and 7 (*C*), and changes in wet weights of, and hemoglobin and PGE_2 levels in, the granulation tissues were quantified (*D*). Values are the mean ± S.E. ($n = 12–13$; *, $p < 0.05$ *versus* replicate KO mice). The time course of expression of COX-2, mPGES-1, VEGF, and HDC by day 5 (*E*) and the expression of COX-1 and mPGES-2 on day 5 (*F*) in the granulation tissues were assessed by immunoblotting. Representative results of more than five experiments are shown in *A*, *C*, *E*, and *F*.

there was no increase in PGE_2 during days 1–3 (Fig. 4*D*, *right panel*). On day 7, the hemoglobin and PGE_2 levels in the granulation tissue of WT mice returned to levels comparable with those of KO mice (Fig. 4*D*).

As assessed by immunoblotting, COX-2 and mPGES-1 were not expressed in the normal dorsum of WT mice (data not shown) and were markedly induced in the granulation tissue formed after cotton thread implantation (Fig. 4*E*). The inducible expression of COX-2 reached a peak on days 1–3 and then declined (Fig. 4*E*), thus roughly coinciding with the levels of PGE_2 in the granulation tissue (Fig. 4*D*, *right panel*). The expression level of COX-2 was slightly higher in WT mice than in KO mice on day 3. The expression of mPGES-1 reached a plateau peak on days 3–5 in WT mice, whereas mPGES-1 was absent from KO mice over the whole period (Fig. 4*E*). Expression of COX-1 and mPGES-2 was unchanged over the experimental period and was similar between WT and KO mice (Fig. 4*F*).

Granulation tissue formation and angiogenesis observed in this model depend on the up-regulation of VEGF, an essential angiogenic factor, and HDC, an enzyme required for the synthesis of histamine (25). We therefore assessed by immunoblotting the expression of VEGF and HDC in the granulation tissue of mPGES-1 KO and WT mice. Although the expression levels of VEGF were similar between WT and KO mice on day 1, there were significant elevations in VEGF expression in WT mice compared with KO mice on days 3–5 (Fig. 4*E*). The expression levels of HDC, which appeared as 70- and 55-kDa forms, were significantly higher in WT mice than in KO mice over the whole experimental periods (Fig. 4*E*). These results suggest that mPGES-1-derived PGE_2 plays an augmentative role in the expression of VEGF and HDC.

Histological analyses of the granulation tissues revealed the presence of a fibroblastic layer around the implanted cotton thread, which was thicker in WT mice than in mPGES-1 KO mice (Fig. 5, *A* and *B*). The smooth muscle layer in WT mice was edematous, an event that was less clear in KO mice (Fig. 5*A*). In addition, more capillary vessels were found in the fibroblastic layer of WT mice than in that of KO mice (Fig. 5*B*). For quantification of capillary vessel formation, we took seven digital images of randomly selected areas of the granulation tissue of WT and KO mice, and the numbers of capillary vessels and the pixels of vessel areas (as an indication of vessel volumes) were evaluated. As a result, the numbers of capillary vessels of WT and KO mice/digital image were 23.3 ± 4.7 and 11.7 ± 1.4 ($p < 0.05$), respectively, and the pixel numbers were 9,800 ± 1,500 and 4,200 ± 750 ($p < 0.05$), respectively, thus revealing ~50% reduction in capillary vessel formation (in terms of both numbers and sizes) in KO mice compared with WT mice. Immunohistochemical staining of these tissues with anti-mPGES-1 antibody showed that mPGES-1 immunoreactivity was distributed mainly in macrophages infiltrating into the fibroblast layer of WT mice (Fig. 5, *C* and *D*). Fewer macrophages were found in replicate KO mice, from which mPGES-1 immunoreactivity was absent.

Participation of mPGES-1 in Inflammatory Arthritis—Experimental and clinical evidence suggests that PGE_2 is a critical mediator of rheumatoid arthritis in humans and in related animal models (36–42). Therefore, we next examined the contribution of mPGES-1 to collagen antibody-induced arthritis

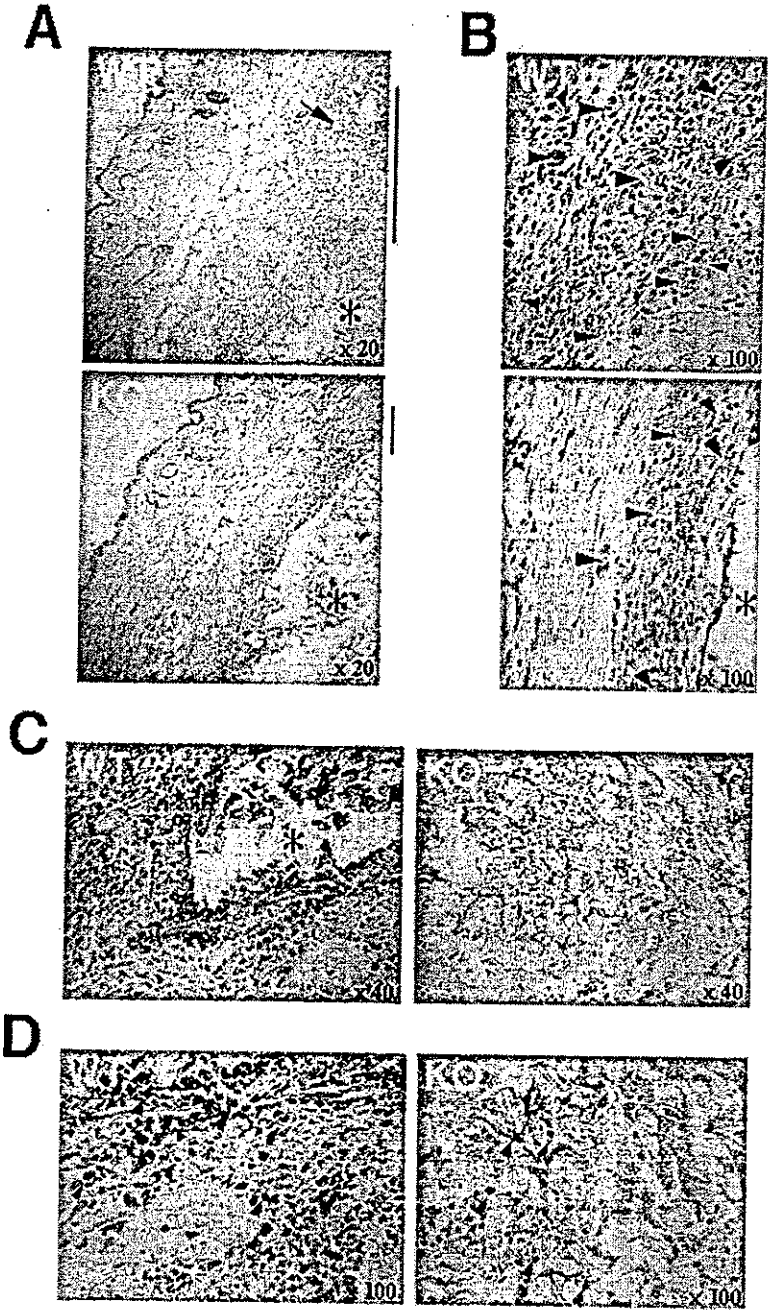

FIG. 5. **Histological analyses of cotton thread-induced granulation tissues.** *A* and *B*, hematoxylin and eosin staining of the 5-day granulation tissues from WT and KO mice at low (*A*) and high (*B*) magnifications. *Arrow* and *asterisks* in *A* indicate the edematous lesion in the smooth muscle layers and the positions of the implanted cotton thread, respectively. *Arrowheads* in *B* indicate capillary vessels in the fibroblastic layers. *C* and *D*, immunohistochemical staining of the granulation tissues with anti-mPGES-1 antibody at low (*C*) and high (*D*) magnifications. Scattered staining of mPGES-1 was found in WT, but not KO, mice. *Asterisk* in *C* indicates the position of the cotton thread, and *arrowheads* in *D* indicate macrophage-like cells.

(CAIA), an experimental animal model for human rheumatoid arthritis. Compared with classical collagen-induced arthritis (CIA), the induction of which is limited to only a few strains such as DBA/1 (43), the CAIA model has the great advantages of applicability to various strains, rapid induction, and high incidence of arthritis. To this end, a mixture of anti-type II collagen monoclonal antibodies was administered to mPGES-1 KO and WT mice with C57BL/6 × 129/SvJ background. However, after application of the antibody mixture plus only one injection of LPS (on day 2), active inflammation declined after 2 weeks so that we were unable to observe obvious bone destruction radiographically (data not shown). We therefore performed booster injections of LPS into these mice every 3 days from day 7, which eventually allowed sustained arthritic inflammation over 4 weeks.

The arthritis score in WT mice began to rise on day 4, reaching a peak value (score ~7) on days 7–10, and then decreased gradually to a still elevated score of >5 by 4 weeks (Fig. 6*A*). Although replicate mPGES-1 KO mice also developed arthritic symptoms during the same period, there was a significant reduction in the severity of the disease in mPGES-1 KO mice compared with WT mice (40~50% reduction from days 7 to 28). In contrast to the reduced severity, however, the incidence of arthritis was 100% in both WT and KO mice. On day 6, when the arthritis was developing (Fig. 6*A*), PGE_2 levels in all four paws of arthritis-induced WT and KO mice were increased significantly over those in their respective saline control groups (Fig. 6*B*). Importantly, there was a ~50% reduction in the PGE_2 level in arthritis-induced KO mice relative to that in replicate WT mice (Fig. 6*B*). As assessed by immunoblotting,

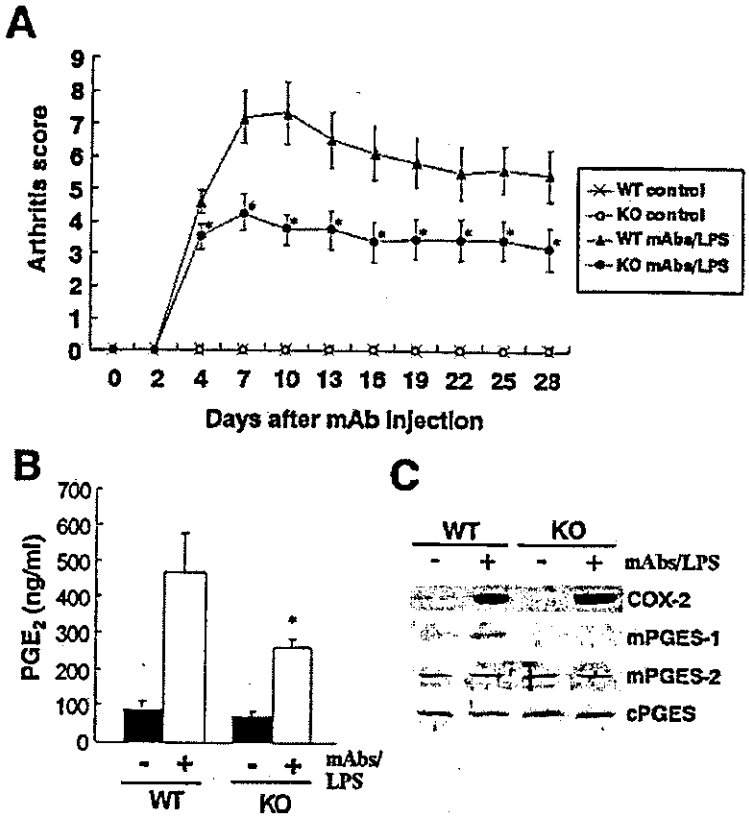

FIG. 6. **Reduced severity of CAIA in mPGES-1 KO mice.** mPGES-1 KO and WT mice were injected with anti-collagen monoclonal antibodies (*mAb*) on day 0 and boosted with LPS on days 2 and 7, followed by intermittent LPS injections every 3 days. *A*, the clinical arthritis score was graded on a 0–3 scale as described under "Experimental Procedures." Values are the mean ± S.E. (n = 10–11; *, $p < 0.05$ *versus* monoclonal antibody/LPS-treated WT mice on each day). *B* and *C*, all four paws of mice in each group were removed on day 6, and homogenized tissues were subjected to PGE_2 measurement (*B*) and Western blotting (*C*). In *B*, values are the mean ± S.E. (n = 3; *, $p < 0.05$ *versus* replicate WT mice).

the expression of COX-2 and mPGES-1 was increased markedly, whereas that of mPGES-2 and cPGES remained unchanged, in arthritis-induced WT mice (Fig. 6*C*). In mPGES-1 KO mice, the inducible expression of COX-2 and constitutive expression of cPGES and mPGES-2 were similar to those in WT mice, whereas mPGES-1 was absent.

Histopathological examination using knee joint sections of arthritis-induced mice on day 28 revealed notable joint destruction in WT mice (Fig. 7*A*, *upper two panels*). Cartilage degeneration was also evident in the toluidine blue-stained sections (Fig. 7*A*, *lower two panels*), which is suggestive of significant proteoglycan loss in articular cartilage of WT mice. In contrast, these histopathological changes were rather mild in arthritis-induced KO mice (Fig. 7*A*, *right panels*). We further compared the arthritis-induced bone loss between the two genotypes by measuring BMD of the periarticular region. The decrease in BMD of diseased WT mice relative to control WT mice was nearly 20%, whereas that of KO mice was only 12%, thereby revealing about 40% less BMD loss in KO mice than in WT mice (Fig. 7*B*).

Fig. 7*C* shows radiographs of forepaws and histologies of the TRAP staining of the metacarpal bones in arthritis-induced WT and KO mice on day 28. Bone erosion and periositis were obvious in WT mice but were not clear in KO mice. Furthermore, histomorphometric parameters of bone resorption, namely osteoclast number and percent eroded surface, were much more increased by arthritis in WT mice than in KO mice (Fig. 7*D*). Collectively, these results indicate that mPGES-1-derived PGE_2 may be involved in development of CAIA and the accompanying joint destruction.

DISCUSSION

In keeping with various pathophysiological roles of PGE_2, as demonstrated by pharmacological inhibition and gene targeting of COX-2 and the four PGE receptors EP1–EP4 (1, 2), we used mPGES-1-deficient mice (20) to evaluate the *in vivo* functions of mPGES-1, a terminal PGE_2-biosynthetic enzyme that is markedly up-regulated during inflammatory responses (3–14). We provide unequivocal evidence that mPGES-1 plays a pivotal role in the production of PGE_2 linked to inflammatory pain hypersensitivity, inflammatory granulation associated with angiogenesis, and inflammatory arthritis accompanying bone destruction. Even though significant PGES enzymatic activity, which may be ascribed to mPGES-2, cPGES, or possibly other as yet unidentified enzymes, still exists in various tissues and cells of mPGES-1 KO mice, mPGES-1 accounts for the majority of the inducible PGES activity (Fig. 1), and importantly, it contributes far more critically to the propagation of inflammatory responses. This conclusion is supported by the facts that mPGES-1 exhibits the highest catalytic activity among the PGES enzymes identified so far (11) and that this enzyme shows preferential, if not strict, coupling selectivity with COX-2, an inducible COX isoform that has been implicated in various inflammatory disorders (4). Our results are in many aspects consistent with a recent report by Audoly and co-workers (44), who also demonstrated reduced pain nociception and inflammatory arthritis in their mPGES-1 KO mice, although there are some subtle differences in the evaluations of the results.

No doubt, PGE_2 is a critical modifier of pain nociception (24, 30, 31). It has been reported that in mice with a mixed genetic background of C57BL/6 × 129/SvJ, the PGI receptor IP mainly mediates immediate pain (30), whereas the PGE receptor EP3, in cooperation with IP, participates in pain hyperalgesia after priming with LPS (24), in the acetic acid-induced writhing model. On the other hand, another study using EP1-deficient mice of the DBA/1 background has demonstrated the striking